

Event Handedness in e^+e^- Annihilation to Three Jets^{*}

Arnd Brandenburg[†]

Institut für Theoretische Physik

Physikzentrum

Rheinisch-Westfälische Technische Hochschule Aachen

52056 Aachen, Germany

Lance Dixon and Yael Shadmi[‡]

Stanford Linear Accelerator Center

Stanford University

Stanford, CA 94309

Abstract

We discuss rescattering effects that can be measured in e^+e^- annihilation to three jets through a single gauge boson, by using triple product (“event handedness”) correlations of the Z (γ^*) polarization with jet momenta. The gauge boson polarization may be produced either by polarized beams or through the natural polarization (left-right asymmetry) of the Z . QCD rescattering does not generate triple product correlations at one loop for massless quarks. We therefore calculate the QCD contribution for massive quarks, as well as the contribution of W and Z exchange loops for massless quarks. Due to various cancellations, the standard model predictions for triple-product correlations at the Z are very small, making such measurements potentially sensitive to physics beyond the standard model. For example, the effects of a new gauge boson that couples only to baryon number may be larger than the standard model contributions; however the effects would probably still be too small to effectively constrain it.

Submitted to Physical Review D

^{*}Research supported by the US Department of Energy under grant DE-AC03-76SF00515.

[†]Research supported in part by the Max Kade Foundation.

[‡]Present address: Fermi National Accelerator Laboratory, P.O. Box 500, Batavia, IL 60510.

1. Introduction

The standard model has withstood experimental scrutiny remarkably well, even as precision measurements at LEP, SLC and the Tevatron are becoming sensitive to electroweak radiative corrections. It is important to test the standard model with as many observables as possible. Observables that vanish identically at tree level are special, in that *any* nonzero measurement of such a quantity simultaneously probes higher-order standard model corrections and potential physics beyond the standard model. Examples of such observables include the GIM-protected processes $K^0 \rightarrow \bar{K}^0$ and $b \rightarrow s\gamma$, as well as many CP-violating quantities.

It is also possible to construct tree-vanishing observables in jet physics. Consider the following observable in e^+e^- annihilation into three jets,

$$\hat{\mathbf{k}}_e \cdot (\mathbf{k}_1 \times \mathbf{k}_2), \quad (1.1)$$

where \mathbf{k}_1 and \mathbf{k}_2 are the momentum vectors of jets 1 and 2, labeled according to the energy-ordering $E_1 > E_2 > E_3$, and $\hat{\mathbf{k}}_e$ is the electron beam direction. A triple product correlation may be defined as the expectation value of (1.1),

$$\langle \hat{\mathbf{k}}_e \cdot (\mathbf{k}_1 \times \mathbf{k}_2) \rangle. \quad (1.2)$$

On the Z pole, (1.2) is proportional to the Z boson polarization, which may be produced either with longitudinally polarized beams (such as the $\sim 60-80\%$ polarized electrons available at SLC [1]), or with unpolarized beams [2], utilizing the natural Z polarization induced by the left-right asymmetry $A_{LR}^{(e)} \sim 14\%$ [1]. In both cases the polarization vector of the Z boson sample points along the beam direction.

In the case of e^+e^- annihilation into a virtual photon, i.e. in the absence of axial vector couplings, one needs longitudinally polarized beams to get a nonzero value of (1.2). This case was first discussed in [3,4].

The observable (1.1) is even under CP, and odd under T_N , where T_N reverses spatial momenta and spin vectors. T_N does not exchange initial and final states, and so it is not the true time reversal operation T . Because of the distinction between T_N and T , a nonzero value of (1.2) does *not* signal CPT violation. It can be produced by final-state rescattering, even in a theory that respects CP and T [5].

There are other variations on (1.1), with the same symmetry properties, which will be discussed in due course. In particular, instead of the expectation value (1.2), one can discuss the asymmetry

associated with it, namely

$$\frac{N(\hat{\mathbf{k}}_{\mathbf{e}} \cdot (\mathbf{k}_1 \times \mathbf{k}_2) > 0) - N(\hat{\mathbf{k}}_{\mathbf{e}} \cdot (\mathbf{k}_1 \times \mathbf{k}_2) < 0)}{N(\hat{\mathbf{k}}_{\mathbf{e}} \cdot (\mathbf{k}_1 \times \mathbf{k}_2) > 0) + N(\hat{\mathbf{k}}_{\mathbf{e}} \cdot (\mathbf{k}_1 \times \mathbf{k}_2) < 0)} . \quad (1.3)$$

where $N(\hat{\mathbf{k}}_{\mathbf{e}} \cdot (\mathbf{k}_1 \times \mathbf{k}_2) > 0)$ is the number of three jet events for which $\hat{\mathbf{k}}_{\mathbf{e}} \cdot (\mathbf{k}_1 \times \mathbf{k}_2) > 0$, etc. In the following, we will use the terms triple product correlation and asymmetry interchangeably.

The large number of polarized Z bosons now available, at both SLC and LEP, allows for sensitive tests of rescattering effects, through measurement of triple product correlations such as (1.2). It is therefore important to calculate the standard model predictions, and that is the main goal of this work.

Triple product correlations in e^+e^- annihilation into jets were also proposed for the study of CP violation [6,7] and (in $e^+e^- \rightarrow W^+W^-$) for the study of weak gauge boson couplings [8].

The triple product correlation (1.2) could also be termed “event handedness”, by analogy to “jet handedness” observables [9] in which $\hat{\mathbf{k}}_{\mathbf{e}}$ is replaced by the axis of a jet produced by a longitudinally polarized parton, and \mathbf{k}_i become momenta of particles inside that single jet, rather than jet momenta. At the event level, as opposed to the jet level, one probes rescattering phases generated at much shorter distance scales, where perturbative techniques may be applied.

In a covariant framework, a nonzero triple product correlation in $e^+e^- \rightarrow$ three jets is produced by terms in the differential cross-section that are proportional to the Levi-Civita tensor $\varepsilon_{\mu\nu\sigma\rho}$ contracted with four of the five momentum vectors in the problem. (Up to a sign, different choices of the four momenta give the same contraction, due to momentum conservation.) The contracted Levi-Civita tensor must be multiplied by the imaginary part of some loop integral, in order to contribute to the differential cross-section.

A first guess for how a triple product correlation might be generated in the standard model is via QCD rescattering of the final-state partons in $e^+e^- \rightarrow (\gamma^*, Z) \rightarrow q\bar{q}q\bar{q}$. Indeed, in crossed channels such as $q\bar{q} \rightarrow g(\gamma^*, Z) \rightarrow g\ell^+\ell^-$, which contribute to Drell-Yan production in (polarized) proton-proton scattering, it has been shown [10,11] that one loop QCD generates a nonvanishing single spin asymmetry, very much like (1.2). Similar effects occur in semi-inclusive deep-inelastic scattering, $e^-p \rightarrow e^-hX$, where h is a single hadron [12].

Amusingly, however, rescattering effects in QCD with massless quarks do *not* generate the triple product correlation at one loop. The various cuts conspire to precisely cancel each other in the fully time-like kinematics of e^+e^- annihilation through a vector boson, unless some of the particles propagating around the loop are massive [12,3]. As we show in appendix I, generalizing an argument due to Körner and Schuler [13], this vanishing holds for $e^+e^- \rightarrow (\gamma^*, Z) \rightarrow n$ -partons at one loop. Though we do not have a proof, we expect — and we will assume here — that the

argument goes through to all orders in α_s perturbation theory for massless partons. We expect the argument to break down at the nonperturbative level, due to the dynamical generation of particle masses in QCD at this level.

In the standard model, there are three possible sources for the particle masses needed to generate the 3-jet triple product correlation:

1) In QCD rescattering, one can include the effects of nonzero quark masses, in diagrams such as figure 1. These effects were first calculated by Fabricius, Kramer, Schierholz and Schmitt [4] in the case of a virtual photon (no quark axial coupling contributions); they presented numerical results for two choices of m_q/\sqrt{s} . At the Z peak, the only significant quark mass is m_b . A naive estimate of the size of the triple product (1.2) generated by the b quark mass in $e^+e^- \rightarrow b\bar{b}g$ is

$$N_c \alpha_s \frac{m_b^2}{M_Z^2} M_Z^2 \approx 10^{-3} M_Z^2, \quad (1.4)$$

where $N_c = 3$ is a color factor, α_s comes from the additional strong coupling constants, beyond those present in the tree-level 3-jet production rate, and $\frac{m_b^2}{M_Z^2}$ reflects the fact that the effect must vanish as $m_b \rightarrow 0$. (It cannot vanish as m_b , since the suppression is a kinematic effect, independent of whether the b is a fermion or a scalar.) Of course the corresponding contribution would be even smaller for u, d, s, c .

2) There is another type of QCD “rescattering” where the massive quark annihilates and is not an external state, first studied by Hagiwara, Kuruma and Yamada [14]. This contribution requires a triangle diagram with two external gluons (see figure 2); due to Furry’s theorem the third vector boson must have an axial coupling to the quark in the triangle loop, i.e. it must be the Z rather than the photon. Naively this contribution is of the same order (1.4), except that it lacks the factor of N_c . Also, it can contribute to non- b final states, so one might expect a compensating factor of $n_f = 5$. However, the relative contributions of up- and down-type quarks in the final state turn out to be opposite in sign and almost equal in magnitude, so one does not get the n_f enhancement, and we will see that this contribution is much smaller than the first one at all energies below the $t\bar{t}$ threshold.

3) A final possibility is electroweak rescattering, the exchange of a W or a Z between the outgoing quark-antiquark pair (see figure 3). In this case the naive estimate is just

$$\alpha_W M_Z^2 \approx \frac{1}{30} M_Z^2. \quad (1.5)$$

Electroweak rescattering can only compete with QCD rescattering because of the quark mass suppression in equation (1.4).

As we show, all of these naive estimates turn out to be overestimates, due largely to phase space factors, and the standard model contributions are quite small. We will also consider one

beyond-the-standard-model effect that might be seen or constrained by this observable. In order to generate a triple-product asymmetry, at least two of the particles propagating around the loop must be on-shell. But if the new particles one wants to probe must be produced on-shell to generate an asymmetry, it may be easier to constrain them based on their direct production rather than by using the asymmetry. Thus, one does not expect large contributions from supersymmetry effects. For example, one loop diagrams involving squarks and gluinos would not contribute to a three-jet asymmetry at the Z pole, since the squark propagators would be off-shell, given current bounds on squark masses. The asymmetries may be more sensitive to the exchange of a single new particle. If a gauge boson B couples to baryon number, and therefore does not couple directly to leptons, then it is hard to detect by other means even if it is as light as 10-20 GeV [15,16]. Yet in this mass range it would give a result like the electroweak result, except potentially scaled up by a large factor, if the coupling constant α_B is larger than the electroweak coupling constant and if the B mass is significantly less than the W and Z masses. The contribution of this hypothetical B boson is simply obtained from the electroweak calculation.

Three types of standard model contributions to the triple product (1.2) in e^+e^- annihilation are *not* investigated in this paper. In the first two, the e^+e^- annihilation does not proceed through a single gauge boson, so the kinematic invariants appearing in the loop integrals are not all timelike. Therefore the argument in appendix I does not apply, and non-vanishing triple product correlations can be generated even when all particle masses are set to zero.

1) The electron-positron annihilation can produce a $\gamma\gamma$ pair, or a γZ pair, which then rescatter into the $q\bar{q}g$ final state. (See figure 4.) This contribution is likely to be very small at the Z pole, because it is proportional to α_{QED} and one does not get the advantage of the Z pole (unless the photon in the γZ intermediate state is very soft).

2) Another possibility is two-photon physics, $\gamma\gamma \rightarrow q\bar{q}g$, where the photons are produced as initial-state radiation. (See figure 5.) At a real $\gamma\gamma$ collider the analogous triple product may be sizable. In e^+e^- annihilation at the Z pole, however, the initial-state radiation is likely to be too small to make this contribution observable.

3) All of the above contributions are those of short-distance physics. In addition there may be long-distance, nonperturbative QCD effects. (Such contributions to spin-momentum correlations in $e^+e^- \rightarrow 4\pi$ were discussed in [17].) These should be suppressed by some power of Λ_{QCD}/\sqrt{s} , but in the absence of an operator product expansion we do not know the precise power, let alone the prefactor. Some nonperturbative effects can be estimated using a hadronization Monte Carlo, but this one seems particularly difficult because of the need to keep track of phases to get the effect.

Finally, we note that the Z width, or more generally, imaginary parts of vacuum polarization

and vertex corrections in the leptonic part of the cross-section, do not contribute to (1.2). These only renormalize the tree amplitude, and therefore, as in the case of the soft singularities discussed in appendix I, cannot generate the triple product asymmetry.

2. Notation

The $e^+e^- \rightarrow (\gamma^*, Z) \rightarrow q\bar{q}g$ differential cross-section at center-of-mass energy \sqrt{s} , assuming no transverse beam polarization, can be written as follows (we adopt the notation of ref. [14]):

$$\begin{aligned} \frac{d^4\sigma}{dx d\bar{x} d\cos\theta d\phi} = \frac{3}{4\pi} \frac{\alpha_s}{\pi} \sigma_{\text{pt}} \times & \left[F_1(1 + \cos^2\theta) + F_2(1 - 3\cos^2\theta) + F_3\cos\theta \right. \\ & + F_4\sin 2\theta\cos\phi + F_5\sin^2\theta\cos 2\phi + F_6\sin\theta\cos\phi \\ & \left. + F_7\sin 2\theta\sin\phi + F_8\sin^2\theta\sin 2\phi + F_9\sin\theta\sin\phi \right], \end{aligned} \quad (2.1)$$

where

$$\sigma_{\text{pt}} = \sigma(e^+e^- \rightarrow \gamma^* \rightarrow \mu^+\mu^-) = \frac{4\pi\alpha^2}{3s}. \quad (2.2)$$

The only kinematic variables appearing in the functions F_i are the scaled quark and antiquark energies in the e^+e^- center-of-mass frame, $x = 2E_q/\sqrt{s}$ and $\bar{x} = 2E_{\bar{q}}/\sqrt{s}$. The angle between the electron direction and the quark direction is θ (see figure 6), and the (signed) angle between the e^+e^-q plane and the $q\bar{q}g$ plane is ϕ . Denote by $\theta_n^{(q\bar{q})}$ the angle between the electron direction and the normal to the $q\bar{q}g$ event plane,

$$\cos\theta_n^{(q\bar{q})} = \frac{\hat{\mathbf{k}}_e \cdot (\mathbf{k}_q \times \mathbf{k}_{\bar{q}})}{|\mathbf{k}_q \times \mathbf{k}_{\bar{q}}|}. \quad (2.3)$$

This angle is related to (θ, ϕ) by

$$\cos\theta_n^{(q\bar{q})} = \sin\theta\sin\phi, \quad (2.4)$$

so the observable (1.1) derives from the function F_9 . Functions F_7 and F_8 are also odd under T_N , but in a CP invariant theory they give vanishing contribution to observables in which the quark and antiquark are not distinguished from each other [7], and so we will not consider them further at this time.

The distribution in the normal angle $\theta_n^{(q\bar{q})}$, after integrating over the remaining angle, is

$$\begin{aligned} \frac{d^3\sigma}{dx d\bar{x} d\cos\theta_n^{(q\bar{q})}} = \frac{3}{2} \frac{\alpha_s}{\pi} \sigma_{\text{pt}} \times & \left[F_1\left(1 + \frac{1}{2}\sin^2\theta_n^{(q\bar{q})}\right) + (F_2 - F_5)\left(1 - \frac{3}{2}\sin^2\theta_n^{(q\bar{q})}\right) \right. \\ & \left. + F_9\cos\theta_n^{(q\bar{q})} \right], \end{aligned} \quad (2.5)$$

We assume that the electrons have longitudinal polarization P_e , with $P_e = +1$ for right-handed electrons, while the positrons are taken to be unpolarized, although polarized positrons can be treated easily as well.

The denominator of the expectation value (1.2) is found (to lowest order in α_s) by integrating the tree approximations to F_1 and $F_2 - F_5$ over the Dalitz plot with some three-jet cut, e.g. on the thrust T or on the invariant masses of parton pairs.

The tree-level approximations to F_i are given by

$$F_i(x, \bar{x}) = g_i^{(0),v} F_i^{(0),v}(x, \bar{x}) + g_i^{(0),a} F_i^{(0),a}(x, \bar{x}) + \mathcal{O}(\alpha_s), \quad (2.6)$$

where the tree-level coupling factors for P-even terms are

$$\begin{aligned} g_i^{(0),v} &= \left((V_e^2 + A_e^2) - 2V_e A_e P_e \right) V_q^2 |\chi(s)|^2 - 2Q(V_e - A_e P_e) V_q \text{Re} \chi(s) + Q^2, \\ g_i^{(0),a} &= \left((V_e^2 + A_e^2) - 2V_e A_e P_e \right) A_q^2 |\chi(s)|^2, \\ g_i^{(0)} &= g_i^{(0),v} + g_i^{(0),a} \\ &= \left((V_e^2 + A_e^2) - 2V_e A_e P_e \right) (V_q^2 + A_q^2) |\chi(s)|^2 - 2Q(V_e - A_e P_e) V_q \text{Re} \chi(s) + Q^2, \\ &i = 1, 2, 4, 5. \end{aligned} \quad (2.7)$$

Here Q is the charge of the quark, V_e , A_e , V_q , A_q are the vector and axial-vector couplings of the Z to the electron and (external) quark,

$$\begin{aligned} V &= \frac{1}{2} I_3 - q \sin^2 \theta_W, & A &= \frac{1}{2} I_3, \\ \chi(s) &= \frac{1}{\sin^2 \theta_W \cos^2 \theta_W} \frac{s}{s - M_Z^2 + i M_Z \Gamma_Z}, \end{aligned} \quad (2.8)$$

with I_3 and q the third component of isospin and charge of the electron or quark.

At or around the Z resonance, it is an excellent approximation to set the external quark masses to zero in the tree cross-section. The kinematic functions are then

$$\begin{aligned} F_1^{(0),v} &= F_1^{(0),a} = \frac{x^2 + \bar{x}^2}{2(1-x)(1-\bar{x})}, \\ F_2^{(0),v} - F_5^{(0),v} &= F_2^{(0),a} - F_5^{(0),a} = 0, \end{aligned} \quad (2.9)$$

and only the coupling $g_1^{(0)}$ contributes in the denominator of (1.2). The full expressions, keeping quark masses, which are needed to estimate the effects at energies below the Z resonance, are more complicated. They are given in appendix II and agree with the results of [18].

3. Contributions to F_9

Now we compile the one loop contributions to $F_9(x, \bar{x})$ from the various sources. All the contributions are proportional to

$$|\mathbf{k}_q \times \mathbf{k}_{\bar{q}}| = \frac{s}{8} \sqrt{(1-x)(1-\bar{x})(x+\bar{x}-1) - z(2-x-\bar{x})^2}, \quad (3.1)$$

so it is convenient to factor out the square-root appearing in (3.1) from the expressions to follow. Note that in the center-of-mass system, it does not matter which two of the outgoing parton momenta appear on the left hand side of (3.1).

1. QCD $e^+e^- \rightarrow (\gamma^*, Z) \rightarrow b\bar{b}g$ Contribution

Write

$$F_{9,\text{QCD}}(x, \bar{x}) = \frac{\alpha_s}{\pi} \sqrt{(1-x)(1-\bar{x})(x+\bar{x}-1) - z(2-x-\bar{x})^2} \left[g_9^{(1),v} f_{\text{QCD}}^v + g_9^{(1),a} f_{\text{QCD}}^a \right], \quad (3.2)$$

where

$$\begin{aligned} g_9^{(1),v} &= \left(-2V_e A_e + (V_e^2 + A_e^2) P_e \right) V_q^2 |\chi(s)|^2 - 2Q(V_e P_e - A_e) V_q \text{Re } \chi(s) + Q^2 P_e, \\ g_9^{(1),a} &= \left(-2V_e A_e + (V_e^2 + A_e^2) P_e \right) A_q^2 |\chi(s)|^2. \end{aligned} \quad (3.3)$$

The functions $f_{\text{QCD}}^v, f_{\text{QCD}}^a$ can be decomposed into leading-color and subleading-color contributions,

$$\begin{aligned} f_{\text{QCD}}^v &= 3 f^{v,1} + \frac{1}{3} f^{v,2}, \\ f_{\text{QCD}}^a &= 3 f^{a,1} + \frac{1}{3} f^{a,2}, \end{aligned} \quad (3.4)$$

whose rather lengthy expressions are given in formulae (II.2) through (II.10) of appendix II.

Numerical results for the vector part of $F_{9,\text{QCD}}$ (in the notation used here), as a function of the thrust and the angle between quark and antiquark momenta, were presented in ref. [4] for two values of m_q/\sqrt{s} . Our results have the opposite sign. The absolute values presented in figure 3 of ref. [4] also differ slightly from ours.

2. QCD $e^+e^- \rightarrow Z \rightarrow g^*g \rightarrow q\bar{q}g$ Contribution

In this case the quarks in the loop may differ from the external quark; denote the internal quark masses by m_i , where i runs over u, d, s, c, b if we are at the Z pole. Write

$$F_{9,Zg^*g}(x, \bar{x}) = \frac{\alpha_s}{\pi} g_{9,Zg^*g}^{(1)} \frac{(\bar{x}-x)(x+\bar{x}-1)}{2(1-x)(1-\bar{x})} \sqrt{(1-x)(1-\bar{x})(x+\bar{x}-1) - z(2-x-\bar{x})^2} \text{Im } f, \quad (3.5)$$

where

$$g_{9,Zg^*g}^{(1)} = \left(2V_e A_e - (V_e^2 + A_e^2) P_e \right) A_q |\chi(s)|^2 \quad (3.6)$$

and

$$\text{Im } f \equiv \sum_{i=\text{flavors}} (2I_3^i) \text{Im } f^i. \quad (3.7)$$

For $4m_i^2 > s$, $\text{Im } f^i = 0$. (The top quark does not contribute in the loop here.) For $4m_i^2 < s$, let $z_i = m_i^2/s$. Then there are two kinematical cases,

$$\begin{aligned} \text{Im } f^i &= \frac{\pi}{4(2-x-\bar{x})^2} \left[4z_i \left(\ln(\sqrt{x+\bar{x}-1} + \sqrt{x+\bar{x}-1-4z_i}) - \ln(1+\sqrt{1-4z_i}) \right) \right. \\ &\quad \left. - \sqrt{1 - \frac{4z_i}{x+\bar{x}-1}} + \sqrt{1-4z_i} \right], \quad x+\bar{x} > 1+4z_i, \\ \text{Im } f^i &= \frac{\pi}{4(2-x-\bar{x})^2} \left[4z_i \left(\ln(\sqrt{4z_i}) - \ln(1+\sqrt{1-4z_i}) \right) + \sqrt{1-4z_i} \right], \quad x+\bar{x} < 1+4z_i. \end{aligned} \quad (3.8)$$

Setting $z = 0$ we recover the results of ref [14]. Note that (3.5) is proportional to the axial coupling of both the internal quark and the final-state quark. In particular, the contributions of the (u, d) and (c, s) isospin doublets in the final state cancel, up to the small effects of mass-splittings. If the final-state flavor is not tagged, one may therefore keep only $b\bar{b}g$ final-state contributions to the triple-product asymmetries.

In the limit of small internal quark mass, $z_i \rightarrow 0$, $\text{Im } f^i$ vanishes like z_i , except for the small kinematical strip where $x+\bar{x} < 1+4z_i$, where $\text{Im } f^i$ is $\mathcal{O}(1)$. If we also neglect the external quark mass (set $z = 0$), then we get

$$\begin{aligned} F_{9,Zg^*g}(x,\bar{x}) &\approx \alpha_s g_{9,Zg^*g}^{(1)} (2I_3^i) z_i \sqrt{\frac{x+\bar{x}-1}{(1-x)(1-\bar{x})}} \frac{(\bar{x}-x) \left((x+\bar{x}-1) \ln(x+\bar{x}-1) + 2-x-\bar{x} \right)}{4(2-x-\bar{x})^2}, \\ &\quad x+\bar{x} > 1+4z_i, \\ &\approx \alpha_s g_{9,Zg^*g}^{(1)} (2I_3^i) \sqrt{\frac{x+\bar{x}-1}{(1-x)(1-\bar{x})}} \frac{(\bar{x}-x)(x+\bar{x}-1)}{8(2-x-\bar{x})^2}, \\ &\quad x+\bar{x} < 1+4z_i. \end{aligned} \quad (3.9)$$

3. Electroweak $e^+e^- \rightarrow (\gamma^*, Z) \rightarrow q\bar{q}g$ Contribution

We neglect all external quark masses in this contribution. Denote the mass of the exchanged vector boson by M_i , $i = Z, W$, and let $\xi_i \equiv M_i^2/s$. At the Z pole, $\xi_Z = 1$, $\xi_W = 0.774$. Write

$$\begin{aligned} F_{9,\text{EW}}(x,\bar{x}) &= -\frac{\alpha}{\sin^2 \theta_W \cos^2 \theta_W} \sqrt{\frac{x+\bar{x}-1}{(1-x)(1-\bar{x})}} \\ &\quad \times \sum_{i=Z,W} g_{9,\text{EW}}^{(1),i} \left[f_{Zq\bar{q}}(\xi_i) + f_{g\bar{q}}(\xi_i) \Theta(1-x-\xi_i) + f_{qg}(\xi_i) \Theta(1-\bar{x}-\xi_i) \right], \end{aligned} \quad (3.10)$$

where $\Theta(y)$ is the Heaviside step function, $\Theta(y) = 0$ for $y < 0$, $\Theta(y) = 1$ for $y > 0$. The function f_{qg} represents the contribution from rescattering in the qg channel (the channel with momentum $k_q + k_g$ flowing through it). Since $(k_q + k_g)^2 > M_t^2$ is required for a nonzero contribution in this channel, only the W contributes to the f_{qg} term, and likewise to the $f_{g\bar{q}}$ term, which arises from rescattering in the $g\bar{q}$ channel. Finally, $f_{Zq\bar{q}}$ comes from the sum of the Z channel (carrying momentum $k_{e^+} + k_{e^-}$) and the $q\bar{q}$ channel contributions; both Z and W contribute here.

The couplings $g_{9,\text{EW}}^{(1),i}$ are given by

$$\begin{aligned} g_{9,\text{EW}}^{(1),i} = & \left((V_q^{(i)})^2 + (A_q^{(i)})^2 \right) \left[\left(-2V_e A_e + (V_e^2 + A_e^2) P_e \right) (V_q^2 + A_q^2) |\chi(s)|^2 \right. \\ & \left. - 2Q(V_e P_e - A_e) V_q \text{Re} \chi(s) + Q^2 P_e \right], \\ & + \left(-2V_e A_e + (V_e^2 + A_e^2) P_e \right) \times 4V_q A_q V_q^{(i)} A_q^{(i)} |\chi(s)|^2, \end{aligned} \quad (3.11)$$

where the Z vector and axial couplings are given by $V_q^{(Z)} = V_q$ and $A_q^{(Z)} = A_q$, as listed in formula (2.8), and the corresponding expressions for W exchange are

$$V_q^{(W)} = A_q^{(W)} = \frac{-1}{2\sqrt{2}} \cos \theta_W, \quad q = u, d, s, c, \quad (3.12)$$

and

$$V_b^{(W)} = A_b^{(W)} = 0. \quad (3.13)$$

In the above we neglect the small off-diagonal CKM matrix elements. The special equation (3.13) is due to the fact that producing a \bar{b} pair after a W exchange requires a $t\bar{t}$ to be present in an intermediate state; but below the $t\bar{t}$ threshold such a graph cannot have an imaginary part.

The kinematic functions are

$$\begin{aligned} f_{Zq\bar{q}}(\xi) = & -\frac{3(1-\bar{x})}{\xi^2} \ell_3\left(\frac{x}{\xi}\right) + \frac{3(1-x)}{\xi^2} \ell_3\left(\frac{\bar{x}}{\xi}\right) \\ & - (1-\bar{x}) \left[\frac{(1-\bar{x})}{\xi(x+\bar{x}-1)} + \frac{2}{\xi^2} \right] \ell_2\left(\frac{x}{\xi}\right) + (1-x) \left[\frac{(1-x)}{\xi(x+\bar{x}-1)} + \frac{2}{\xi^2} \right] \ell_2\left(\frac{\bar{x}}{\xi}\right) \\ & + \frac{(1-\bar{x})^2}{(x+\bar{x}-1)(x+\bar{x}-1+\xi)} \ell_2\left(\frac{1-\bar{x}}{x+\bar{x}-1+\xi}\right) \\ & - \frac{(1-x)^2}{(x+\bar{x}-1)(x+\bar{x}-1+\xi)} \ell_2\left(\frac{1-x}{x+\bar{x}-1+\xi}\right), \end{aligned} \quad (3.14)$$

$$\begin{aligned}
f_{g\bar{q}}(\xi) = & \frac{3(1-\bar{x})(1-x-\xi)^4}{\xi^2} \ell_3\left(\frac{x(1-x-\xi)}{\xi}\right) + \frac{(2-\xi)(1-\bar{x})(1-x-\xi)^3}{\xi^2} \ell_2\left(\frac{x(1-x-\xi)}{\xi}\right) \\
& + \frac{(1-\bar{x})(1-x-\xi)^2}{x+\bar{x}-1} \ell_1\left(\frac{x(1-x-\xi)}{\xi}\right) \\
& - \frac{(x+\xi)(x+\bar{x}-1)(1-x-\xi)^2}{\xi(1-x)} \ell_1\left(\frac{(1-x-\xi)(x+\bar{x}-1)}{\xi}\right) \\
& + \frac{(x+\bar{x}-1+\xi)^2}{(1-\bar{x})(x+\bar{x}-1)} \ln\left(\frac{\xi+(1-x-\xi)(x+\bar{x}-1)}{(x+\xi)(1-x)}\right) \\
& - (1-x-\xi) \left[\frac{(1-x)(1-\bar{x})}{\xi} - \frac{\xi}{x+\bar{x}-1} + \frac{x(1-x-\xi)}{(1-x)^2} - \frac{\xi(1+\bar{x})+2\bar{x}}{2(1-x)} - \frac{3}{2}(1-\bar{x}) \right],
\end{aligned} \tag{3.15}$$

$$f_{qg}(\xi) = -f_{g\bar{q}}(\xi)|_{x \leftrightarrow \bar{x}}, \tag{3.16}$$

where

$$\begin{aligned}
\ell_1(y) &= \frac{\ln(1+y) - y}{y^2}, \\
\ell_2(y) &= \frac{\ln(1+y) - y + y^2/2}{y^3}, \\
\ell_3(y) &= \frac{\ln(1+y) - y + y^2/2 - y^3/3}{y^4}.
\end{aligned}$$

Note that the $\ell_i(y)$ are nonsingular as $y \rightarrow 0$.

4. Non-standard-model “B” Gauge Boson Exchange Contribution

As in the electroweak case, we neglect all external quark masses. Denote the mass of the exchanged vector boson by M_B , and following the conventions of [15,16], let it couple vectorially to quarks with strength $\alpha_B/9$ (since quarks have baryon number 1/3). Let $\xi_B \equiv M_B^2/M_Z^2$. Then the electroweak formulas can be modified to give,

$$\begin{aligned}
F_{9,B}(x, \bar{x}) = & -\frac{\alpha_B}{9} \sqrt{\frac{x+\bar{x}-1}{(1-x)(1-\bar{x})}} \\
& \times g_{9,B}^{(1)} \left[f_{Zq\bar{q}}(\xi_B) + f_{g\bar{q}}(\xi_B) \Theta(1-x-\xi_B) + f_{qg}(\xi_B) \Theta(1-\bar{x}-\xi_B) \right].
\end{aligned} \tag{3.17}$$

The couplings $g_{9,B}^{(1)}$ are now given by

$$g_{9,B}^{(1)} = \left(-2V_e A_e + (V_e^2 + A_e^2) P_e \right) (V_q^2 + A_q^2) |\chi(s)|^2 - 2Q(V_e P_e - A_e) V_q \text{Re} \chi(s) + Q^2 P_e, \tag{3.18}$$

and the functions $f_{Zq\bar{q}}(\xi)$, $f_{g\bar{q}}(\xi)$, $f_{qg}(\xi)$ are exactly as in (3.14)–(3.16).

4. Numerical Results

In this section, we present numerical results for the sizes of the triple product correlations, and their dependence on the center-of-mass energy and the three-jet cut. These results are obtained by

identifying jet momenta with parton momenta. Several different “event handedness” correlations can be constructed for the process we are considering. Here we discuss the different contributions of section 3 to the triple product correlation introduced in (1.2), $\langle \hat{\mathbf{k}}_e \cdot (\mathbf{k}_1 \times \mathbf{k}_2) \rangle$, and the expectation value of the normal angle, as signed by the two fastest jets,

$$\cos \theta_n = \frac{\hat{\mathbf{k}}_e \cdot (\mathbf{k}_1 \times \mathbf{k}_2)}{|\mathbf{k}_1 \times \mathbf{k}_2|}, \quad (4.1)$$

where \mathbf{k}_i are the energy-ordered momentum vectors ($E_1 > E_2 > E_3$). As the two observables are qualitatively similar, we only give numerical results for $\langle \cos \theta_n \rangle$. Other variations, such as $\hat{\mathbf{k}}_e \cdot (\mathbf{k}_1 \times \mathbf{k}_2) / (|\mathbf{k}_1| |\mathbf{k}_2|)$, lead to similar or smaller signals.

The normal angle θ_n , defined by the energy ordering, is equal to the normal angle $\theta_n^{(q\bar{q})}$, defined by the quark and anti-quark, up to a sign

$$\eta = \text{sign}\left((x - \bar{x})(x - x_g)(\bar{x} - x_g)\right), \quad (4.2)$$

where $x_g = 2 - x - \bar{x}$ is the gluon energy fraction.

Performing the angular integrals, the $\cos \theta_n$ expectation value is expressed in terms of F_9 and F_1 by

$$\langle \cos \theta_n \rangle = \frac{1}{4} \frac{\int_{D_c} dx d\bar{x} \eta F_9(x, \bar{x})}{\int_{D_c} dx d\bar{x} F_1(x, \bar{x})}, \quad (4.3)$$

where D_c is the domain in (x, \bar{x}) after making some kind of a three-jet cut. Similarly,

$$\langle \hat{\mathbf{k}}_e \cdot (\mathbf{k}_1 \times \mathbf{k}_2) \rangle = \frac{s}{8} \frac{\int_{D_c} dx d\bar{x} \eta \sqrt{(1-x)(1-\bar{x})(x+\bar{x}-1) - z(2-x-\bar{x})^2} F_9(x, \bar{x})}{\int_{D_c} dx d\bar{x} F_1(x, \bar{x})}. \quad (4.4)$$

On the Z pole, the asymmetries (4.3) and (4.4) are proportional to the Z polarization,

$$P_Z = \frac{P_e - A_{LR}^{(e)}}{1 - P_e A_{LR}^{(e)}}, \quad (4.5)$$

where $A_{LR}^{(e)} = 2V_e A_e / (V_e^2 + A_e^2)$. For example, at $s = M_Z^2$,

$$\begin{aligned} & \langle \hat{\mathbf{k}}_e \cdot (\mathbf{k}_1 \times \mathbf{k}_2) \rangle_{\text{QCD}} \\ &= P_Z \frac{\alpha_s}{\pi} \frac{M_Z^2}{8} \frac{\int_{D_c} dx d\bar{x} \eta \left((1-x)(1-\bar{x})(x+\bar{x}-1) - z(2-x-\bar{x})^2 \right) \left(V_q^2 f_{\text{QCD}}^v + A_q^2 f_{\text{QCD}}^a \right)}{\left(V_q^2 + A_q^2 \right) \int_{D_c} dx d\bar{x} F_1^{(0),v}}. \end{aligned} \quad (4.6)$$

Through most of our analysis, we use the standard cut $y_{ij} \geq y_{\text{cut}}$, where $y_{ij} \equiv (k_i + k_j)^2 / M_Z^2$. Then, for massless quarks D_c is given by

$$D_c : \quad x \leq 1 - y_{\text{cut}}, \quad \bar{x} \leq 1 - y_{\text{cut}}, \quad x + \bar{x} \geq 1 + y_{\text{cut}}.$$

With this cut, and if one neglects quark masses, the leading order contribution to F_1 can be integrated analytically,

$$\begin{aligned}
I_D(y_{\text{cut}}) &\equiv \int_{D_c} dx d\bar{x} F_1^{(0),v}(x, \bar{x}) = \int_{D_c} dx d\bar{x} \frac{x^2 + \bar{x}^2}{2(1-x)(1-\bar{x})} \\
&= \ln^2\left(\frac{1-y_{\text{cut}}}{y_{\text{cut}}}\right) - \frac{3}{2}(1-2y_{\text{cut}}) \ln\left(\frac{1-2y_{\text{cut}}}{y_{\text{cut}}}\right) + 2 \text{Li}_2\left(\frac{y_{\text{cut}}}{1-y_{\text{cut}}}\right) \\
&\quad - \frac{\pi^2}{6} + \frac{5}{4} - 3y_{\text{cut}} - \frac{9}{4}y_{\text{cut}}^2.
\end{aligned} \tag{4.7}$$

We evaluate the remaining x, \bar{x} integrals numerically. As input for our results we use $\alpha_s(M_Z) = 0.116$, $m_b = 4.5$ GeV, $\sin^2 \theta_W = 0.232$, $M_Z = 91.17$ GeV and $M_W = 80.1$ GeV. We always assume complete right-handed electron polarization: $P_e = +1$. It is easy to scale the results to other values of P_e at the Z pole (using equation (4.5)) and well below the Z pole (where the observables are directly proportional to P_e).

At the Z -pole and below it, the largest standard model effects arise from the QCD contribution of section 3.1, which is dominated (for $\sqrt{s} > 2m_b$) by the $b\bar{b}g$ final state. The $F_{9,\text{QCD}}$ contribution to $\langle \cos \theta_n \rangle$ is shown in figure 7 as a function of the center-of-mass energy \sqrt{s} , with $y_{\text{cut}} = 0.04$, for b production only. If the final state is not flavor tagged, then one should average over final state flavors, and the result would be diluted by the fraction of hadronic events containing b quarks. (At the Z , the b fraction is $R_b = \Gamma_b/\Gamma_{\text{hadron}} \approx 0.22$.)

As expected, the signal decreases with increasing s , roughly as m_b^2/s . A further suppression arises because the vector and axial components of the signal have opposite signs. The dotted line shows the vector component of the result, obtained by setting the $Zb\bar{b}$ axial coupling to zero. At small energies, the signal is dominated by the vector component, which is positive. At larger energies, the axial component sets in with an opposite sign, and exactly cancels the vector component just below the Z mass. At energies above the Z mass, the signal is dominated by the axial component. Notice that for center of mass energies below 30 GeV, one would have to increase y_{cut} in order to effectively cut soft gluons, since y_{ij} is always larger than m_b^2/s .

Near the Z pole, the combined W and Z exchange contribution to $\langle \cos \theta_n \rangle$ (from $F_{9,\text{EW}}$), is about +30% of the QCD contribution in an untagged sample. This is partly due to the n_f enhancement of the electroweak contribution; all final state flavors contribute to the asymmetry (except the b in W exchange), whereas, practically, only b quarks contribute in the QCD case. The resulting $\langle \cos \theta_n \rangle$, assuming b quarks are not tagged, and summing over all flavors contributing to the asymmetry in the electroweak contributions, is shown in figure 8 for \sqrt{s} of 70–200 GeV. For high energies, the W exchange contribution becomes dominant. However, recall that we have neglected the contributions with $\gamma\gamma$ and γZ intermediate states (figure 4); and above the W -pair threshold,

additional diagrams with WW intermediate states will contribute as well. At these energies, pure hadronic decays of real W pairs will form a large “background” to the measurement. (Triple product correlations in $e^+e^- \rightarrow W^+W^-$ via electroweak rescattering are discussed in ref. [8].) Here we only plot the center-of-mass energy dependence of the particular contributions we studied.

The second type of QCD rescattering, via the Zg^*g effective vertex discussed in section 3.2, gives rise to asymmetries that are two to three orders of magnitude smaller than the contributions mentioned above. At the Z , with $y_{\text{cut}} = 0.04$ for example, $\langle \cos \theta_n \rangle_{Zg^*g} = -0.95 \times 10^{-8}$. We therefore neglect this contribution in the remainder of the section.

As can be seen, the standard model prediction for the asymmetry at the Z is tiny. One might wonder whether it would change significantly with the choice of the three-jet cut. The T_N -odd correlations should be small both for large values of y_{cut} , which imply an almost symmetric three-jet event, and for small values of y_{cut} , which include soft or collinear regions, where the event is two-jet like. Indeed, at the Z , the QCD contribution to $\langle \cos \theta_n \rangle$ peaks slightly below $y_{\text{cut}} = 0.02$, and the electroweak contributions peak near $y_{\text{cut}} = 0.04$.

However, the relevant quantities to consider in order to determine the optimal cut are not the values of the observables themselves, but rather the corresponding signal-to-noise ratios, which describe the statistical significance of a measurement. The noise comes from root-mean-square fluctuations in the T_N -even cross-section. At lowest-order in α_s (tree-level), and neglecting quark masses, these can be calculated analytically. We find,

$$\Delta \cos \theta_n \equiv \sqrt{\langle \cos^2 \theta_n \rangle - \langle \cos \theta_n \rangle^2} \approx \sqrt{\langle \cos^2 \theta_n \rangle} = \sqrt{\frac{3}{10}}, \quad (4.8)$$

and

$$\begin{aligned} \Delta \hat{\mathbf{k}}_e \cdot (\mathbf{k}_1 \times \mathbf{k}_2) &\approx \sqrt{\langle (\hat{\mathbf{k}}_e \cdot (\mathbf{k}_1 \times \mathbf{k}_2))^2 \rangle} \\ &= \frac{s}{20} \sqrt{\frac{3(1 - 3y_{\text{cut}})^2(2 - 3y_{\text{cut}} + 4y_{\text{cut}}^2 + y_{\text{cut}}^3)}{2I_D(y_{\text{cut}})}}. \end{aligned} \quad (4.9)$$

The corresponding signal-to-noise (S/N) ratio for $\langle \cos \theta_n \rangle$, is then given by

$$S/N(\cos \theta_n) \equiv \frac{|\langle \cos \theta_n \rangle|}{\Delta \cos \theta_n} \sqrt{N_{3\text{-jet}}},$$

and similarly for the triple product, where $N_{3\text{-jet}}$ is the number of three-jet events in the data sample.

The signal-to-noise ratios for $\langle \cos \theta_n \rangle$, from QCD and electroweak rescattering at the Z , are shown in figure 9 as functions of y_{cut} . In the range shown, the ratios increase monotonically as y_{cut} decreases. They eventually start to fall off as expected, but this happens for very low values of the cut, where the perturbative calculation cannot be trusted. It is easy to understand why the S/N

ratio peaks at a lower y_{cut} as does $\langle \cos \theta_n \rangle$. The F_9 integrals are finite for small y_{cut} , whereas the F_1 integrals diverge as double logarithms for massless quarks, or logarithmically for b production. (The b mass cuts off the collinear divergences). The signal to noise ratio is proportional to the F_9 integral divided by the *square root* of the F_1 integral, and so falls off more slowly than $\langle \cos \theta_n \rangle$ for small y_{cut} . The QCD signal-to-noise ratio continues to grow down to $y_{\text{cut}} = 0.003$, even though the F_9 integral is finite in the soft gluon region. This suggests that it receives large contributions in regions where two of the jets are close to collinear. We will return to this point later. We note that replacing y_{cut} by a cut on the smallest jet energy leads to a smaller asymmetry.

We now turn to the effects of the hypothetical B -boson of section (3.4). The contribution of the B boson to $\langle \cos \theta_n \rangle$ at the Z , is given by the solid line in figure 10, as a function of $\xi = m_B^2/M_Z^2$. Here we take the B coupling to be $\alpha_B = 0.2/9$. Up to overall factors which involve the couplings, the Z and W contributions can be read off this plot, at $\xi = \xi_Z = 1$ and $\xi = \xi_W = 0.774$ respectively. The asymmetry is most sensitive to the B boson if its mass is around 25–30 GeV. But even for a mass in this range the signal is probably too small to be observed ($\langle \cos \theta_n \rangle \sim 3 \times 10^{-5}$ or less).

The asymmetries (4.3) and (4.4) involve integrating F_9 with the sign η . Kinematic regions with different energy orderings contribute with different signs and potentially cancel each other. Such cancellations would be avoided if the gluon jet could be identified, so that the asymmetries could be defined according to the energy ordering of the q, \bar{q} jets only. (For example, taking k_1, k_2 in (1.1) to be the q, \bar{q} momenta, with $E_1 > E_2$, so that $\eta = \text{sign}(x - \bar{x})$ in (4.2).) This leads to little improvement for the QCD contribution: $\langle \cos \theta_n \rangle$ hardly changes, and $\langle \hat{\mathbf{k}}_e \cdot (\mathbf{k}_1 \times \mathbf{k}_2) \rangle$ increases by a factor of two to three, depending on the cut. The effect is more significant for the electroweak and hypothetical B -boson contributions to the asymmetries, which increase by a factor of around six. The B -boson contribution to $\langle \cos \theta_n \rangle$ at the Z , assuming the gluon jet is identified, is given by the dashed line in figure 10. Without gluon identification, the maximum signal-to-noise ratio obtained is $0.17\sqrt{\mathcal{L}/\text{fb}^{-1}}$, where \mathcal{L} is the integrated luminosity in inverse femtobarns. If the gluon is identified with efficiency ϵ_g , this becomes $0.6\sqrt{\epsilon_g \mathcal{L}/\text{fb}^{-1}}$, assuming 100% purity.

Another way of enhancing the asymmetry is to use an “optimized” observable [19], i.e., an observable that maximizes the signal-to-noise ratio. If the identity of the particles making up the jets is not known, then the optimized observable is given by:

$$\tilde{O}(x_1, x_2) = \frac{\cos \theta_n}{(\frac{3}{2} - \frac{1}{2} \cos^2 \theta_n)} \times \frac{\sum_{p=1}^6 \eta_p F_9(x_p, \bar{x}_p)}{\sum_{p=1}^6 F_1(x_p, \bar{x}_p)}, \quad (4.10)$$

where x_1, x_2 are the energy fractions of the highest energy and intermediate energy jet respectively, p sums over the six different ways of assigning x_1, x_2 , and $2 - x_1 - x_2$ to x, \bar{x} and $x_g = 2 - x - \bar{x}$, and η_p is η of (4.2), evaluated with $x = x_p, \bar{x} = \bar{x}_p$.

The optimized observable signal-to-noise ratios are only 20–30% bigger than the $\langle \cos \theta_n \rangle$ signal-to-noise ratios for the W , Z and B -boson exchange contributions. This holds whether or not the gluon is identified. The same enhancement occurs for the QCD contribution, with no gluon identification. If the gluon is identified, the enhancement is much bigger. As mentioned above, the QCD asymmetries receive large contributions from regions where two of the jets are close to collinear. An “upper limit” estimation of the signal-to-noise that can be produced by the QCD contribution at the Z is obtained by studying the optimized observable, assuming gluon identification, and replacing y_{cut} by a cut on the jet energies: $E_i \geq E_{\text{min}}$. For $E_{\text{min}} = 5 - 10$ GeV we find, for b production only,

$$\frac{\langle \tilde{O} \rangle}{\langle \tilde{O}^2 \rangle^{1/2}} = (1.5 - 1.9) \times 10^{-4} \quad \text{and} \quad \frac{\langle \cos \theta_n \rangle}{\langle \cos^2 \theta_n \rangle^{1/2}} = (0.6 - 1.0) \times 10^{-4} ,$$

giving signal-to-noise ratios of about

$$S/N(\tilde{O}) = 0.33 \sqrt{\epsilon_g \epsilon_b} \sqrt{\mathcal{L}/\text{fb}^{-1}} \quad \text{and} \quad S/N(\cos \theta_n) = 0.15 \sqrt{\epsilon_g \epsilon_b} \sqrt{\mathcal{L}/\text{fb}^{-1}} ,$$

where ϵ_g , ϵ_b are the gluon identification and b -tagging efficiencies.

Somewhat higher sensitivity to the QCD-induced asymmetry can be achieved at low center-of-mass energies. For $\sqrt{s} = 30$ GeV, the signal-to-noise ratio for $\langle \cos \theta_n \rangle$, with $y_{\text{cut}} = 0.04$, is $0.3 \sqrt{\epsilon_b} \sqrt{\mathcal{L}/\text{fb}^{-1}}$, assuming that the b is tagged with efficiency ϵ_b and 100% purity. With gluon identification, this result becomes $0.4 \sqrt{\epsilon_b \epsilon_g} \sqrt{\mathcal{L}/\text{fb}^{-1}}$. If y_{cut} is replaced by $E_i \geq 2$ GeV, one finds $S/N(\cos \theta_n) = 0.55 \sqrt{\epsilon_b \epsilon_g} \sqrt{\mathcal{L}/\text{fb}^{-1}}$, and $S/N(\tilde{O}) = 0.7 \sqrt{\epsilon_b \epsilon_g} \sqrt{\mathcal{L}/\text{fb}^{-1}}$. In any case, integrated luminosities in at least the tens of inverse-femtobarn range will be required for measurements of these standard model contributions to be statistically significant.

5. Conclusions

Beam polarization, or the natural Z polarization, can be used to construct “event handedness” correlations in $e^+e^- \rightarrow 3\text{-jets}$ that are directly sensitive to rescattering effects. In this paper we have identified and calculated the dominant standard model contributions to several such correlations in e^+e^- annihilation at or below the Z pole.

QCD rescattering of massless quarks does not produce any “event handedness” correlations at one loop in the purely time-like kinematics of e^+e^- annihilation through a single gauge boson. The dominant standard model contributions to these correlations are therefore produced by QCD rescattering of massive quarks, which is suppressed by m_b^2/M_Z^2 at the Z resonance, and by electroweak rescattering, via W and Z exchange loops. We have presented analytic results for the

different contributions. We have studied the dependence of the resulting asymmetries on different kinematic variables of the process considered, including the center-of-mass energy and the three-jet cut. Due to various cancellations, the standard model does not generate large effects; even for “optimized observables” the signal-to-noise ratios are quite small.

Thus, a measurement of event handedness correlations may serve as a probe of physics beyond the standard model and/or nonperturbative effects in jet physics.

We have investigated the asymmetry generated in quark rescattering through the exchange of a hypothetical gauge boson, coupling to baryon number only. The effects are the largest, but would still be difficult to observe, if the mass of this boson lies in the range of 25–30 GeV.

Note added

The SLD collaboration has recently placed an experimental upper bound on the magnitude of $\langle \cos \theta_n \rangle$ at the Z pole, obtaining 95% C.L. limits of $-0.022 < \beta < 0.039$, where $\beta = \frac{16}{9} \frac{1}{P_Z} \langle \cos \theta_n \rangle$ [20].

Acknowledgements

We thank M. Peskin for many useful discussions, and for his careful reading of the paper. We also thank J.D. Bjorken and D. Atwood for useful discussions, and T. Maruyama and P. Burrows for suggesting this work, for continual encouragement and for their comments on the manuscript. A.B. would also like to thank W. Bernreuther for many clarifying discussions.

Appendix I. Vanishing of Event Handedness Correlations in Massless QCD

In this appendix we show that the one-loop QCD contribution to triple-product correlations in e^+e^- annihilation through a single gauge-boson vanishes, unless some of the partons propagating around the loop are massive. This argument generalizes to n -parton final states a previous argument by Körner and Schuler [13] for the three-parton case, $e^+e^- \rightarrow q\bar{q}g$.

A nonzero triple-product correlation is produced by terms in the differential cross-section that are proportional to the Levi-Civita tensor $\varepsilon_{\mu\nu\sigma\rho}$ contracted with four of the five momentum vectors in the problem. The contraction must be multiplied by the imaginary part of some loop integral, in order to contribute to the differential cross-section.

The loop integrals may be defined by analytic continuation from the unphysical, Euclidean region, to the physical region. Denote the external kinematic invariants by $s_{ij} = (k_i + k_j)^2$, with k_i the momentum of the i -th particle. All the s_{ij} are negative in the Euclidean region, and all loop integrals are manifestly real there. Upon going into the physical region, some of the invariants may change sign, and the integrals may develop imaginary parts. However, the dependence of the integrals on the kinematic invariants is through analytic functions of dimensionless ratios, of the form $f(\frac{-s_{ij}}{-s_{kl}})$. The kinematics of e^+e^- annihilation through a single gauge boson is purely timelike — all the invariants appearing in the loop integrals are positive in the physical region. Therefore, ratios of invariants do not change sign upon going from the Euclidean region to the physical region. As a result, the integrals do not develop any imaginary parts in the physical region, and the loop amplitude has no absorptive part.

This ceases to be true if some particle propagating around the loop has a non-zero mass M . In this case the dimensionless functions appearing in the amplitude are of the form $f(\frac{-s_{ij}}{-s_{jk}}, \frac{M^2}{-s_{ij}})$. Since M^2 is positive in both the Euclidean region and the physical region, the ratios $\frac{M^2}{-s_{ij}}$ flip sign as one goes from Euclidean to physical, and imaginary parts are now permitted.

In the above, we ignored one source of a “mass scale”, which is present in perturbation theory even when all the particles are massless, namely, the renormalization scale μ . The renormalized one-loop amplitude for producing n final state partons, $A_n^{1\text{-loop}}$, can be written as a sum of two pieces: an infrared-divergent piece, and a leftover finite piece. (This separation has some arbitrariness associated with it.) The finite piece of $A_n^{1\text{-loop}}$ depends only on the kinematic invariants s_{ij} and on particle masses, and as we saw above, it has no absorptive part in the purely time-like kinematics of the process we are considering. In contrast, the infrared-divergent piece of $A_n^{1\text{-loop}}$ contains logarithms of the form $\ln(\mu^2/(-s_{ij}))$, which may and do develop imaginary parts in physical regions, including the fully time-like region. But, as we now show, these imaginary parts do not contribute to the cross-section at one loop.

When interfered with A_n^{tree} , the infrared-divergent piece of $A_n^{1\text{-loop}}$ cancels soft and collinear phase-space integrations of the tree-level cross-section $|A_{n+1}^{\text{tree}}|^2$ for producing $n+1$ partons, where one of the partons is unobserved. Its form can therefore be inferred from the soft and collinear structure of the cross-section for producing $n+1$ partons. It can be written as a sum of terms, where each term is given by a corresponding term in the tree amplitude A_n^{tree} , multiplied by a factor that depends on a single invariant s_{ij} (see for example [21]). This factor is universal — it only depends on the identity of partons i and j , i.e., on whether they are quarks or gluons.

The strongest singularities come from overlapping soft and collinear regions, and can be written, using dimensional regularization with $D = 4 - 2\epsilon$, as [21]

$$\mathcal{A}_{c_1 \dots c_n}^{1\text{-loop, soft}} = \gamma \sum_{i < j} S_{ij} t_{c_i c'_i}^a t_{c_j c'_j}^a A_{c_1 \dots c'_i \dots c'_j \dots c_n}^{\text{tree}}, \quad (\text{I.1})$$

where c_i is the color index of the i -th parton, t^a are the $SU(N)$ generators, γ is a real constant, and

$$S_{ij} = \frac{1}{\epsilon^2} \left(\frac{\mu^2}{-s_{ij}} \right)^\epsilon. \quad (\text{I.2})$$

When expanded around $\epsilon = 0$, the factor S_{ij} contains the logarithm $\ln(\mu^2/(-s_{ij}))$ which develops an imaginary part in the physical region.

But for each term that contains S_{ij} in the interference $A_n^{1\text{-loop}} A_n^{\text{tree}*}$, there corresponds an identical term in $A_n^{1\text{-loop}*} A_n^{\text{tree}}$, in which S_{ij} is replaced by S_{ij}^* . The imaginary part of S_{ij} therefore drops out in the cross-section. Specifically, the interference $A_n^{1\text{-loop}} A_n^{\text{tree}*}$ contains the term

$$S_{ij} t_{c_i c'_i}^a t_{c_j c'_j}^a A_{c_1 \dots c'_i \dots c'_j \dots c_n}^{\text{tree}} (A_{c_1 \dots c_n}^{\text{tree}})^*, \quad (\text{I.3})$$

while the interference $A_n^{\text{tree}} A_n^{1\text{-loop}*}$ contains the term

$$A_{c_1 \dots c_n}^{\text{tree}} \left(S_{ij} t_{c_i c'_i}^a t_{c_j c'_j}^a A_{c_1 \dots c'_i \dots c'_j \dots c_n}^{\text{tree}} \right)^* = S_{ij}^* t_{c_i c'_i}^a t_{c_j c'_j}^a (A_{c_1 \dots c_n}^{\text{tree}})^* A_{c_1 \dots c'_i \dots c'_j \dots c_n}^{\text{tree}}, \quad (\text{I.4})$$

where in the last line we used the hermiticity of t^a to exchange $c_i \leftrightarrow c'_i$, $c_j \leftrightarrow c'_j$. Thus, only the real part of S_{ij} contributes in the sum of (I.3) and (I.4).

This argument can be repeated for the hard collinear singularities, which have the simpler form

$$\mathcal{A}_{c_1 \dots c_n}^{1\text{-loop, coll}} = \sum_{i < j} \gamma_{ij} \frac{1}{\epsilon} \left(\frac{\mu^2}{-s_{ij}} \right)^\epsilon A_{c_1 \dots c_n}^{\text{tree}}, \quad (\text{I.5})$$

where again $c_1 \dots c_n$ are the color indices of the partons and γ_{ij} are real constants that depend on the identity of partons i and j .

Notice that the argument does not rely on the fact that (I.3) and (I.4) contain the interference of two tree amplitudes. The amplitudes appearing on the two sides of the interference could in

principle be different — the crucial point is that the singular factor can appear on the two sides of the interference, multiplying the same structure. It appears possible to generalize this argument beyond one loop, but we have not yet done so.

Appendix II. Kinematic Functions for QCD Massive Quark Contributions

In this appendix we give the kinematic functions that contribute to the tree-level denominator of the expectation value (1.2), keeping the quark mass nonzero [18], followed by the functions appearing in the one-loop QCD $(\gamma^*, Z) \rightarrow b\bar{b}g$ contribution to F_9 . In both cases we define $z = m_q^2/s$ with m_q the external quark mass.

The tree-level $e^+e^- \rightarrow q\bar{q}g$ kinematic functions appearing in (2.6) are

$$\begin{aligned}
F_1^{(0),v} &= \frac{x^2 + \bar{x}^2}{2(1-x)(1-\bar{x})} + \frac{z(2x\bar{x}(x+\bar{x}) - 3x^2 - 3\bar{x}^2 + 8(x+\bar{x}-x\bar{x}) - 6)}{(1-x)^2(1-\bar{x})^2} \\
&\quad - \frac{2z^2(2-x-\bar{x})^2}{(1-x)^2(1-\bar{x})^2}, \\
F_1^{(0),a} &= \frac{x^2 + \bar{x}^2}{2(1-x)(1-\bar{x})} \\
&\quad + \frac{z(-(x+\bar{x})^2(x+\bar{x}-x\bar{x}) + 8(x^2(1-\bar{x}) + \bar{x}^2(1-x)) + 24x\bar{x} - 12(x+\bar{x}) + 4)}{(1-x)^2(1-\bar{x})^2} \\
&\quad + \frac{4z^2(2-x-\bar{x})^2}{(1-x)^2(1-\bar{x})^2}, \\
F_2^{(0),v} - F_5^{(0),v} &= \frac{2z((1-x)(1-\bar{x})(x+\bar{x}-1) - z(2-x-\bar{x})^2)}{(1-x)^2(1-\bar{x})^2}, \\
F_2^{(0),a} - F_5^{(0),a} &= \frac{z(2-x-\bar{x})^2}{(1-x)^2(1-\bar{x})^2},
\end{aligned} \tag{II.1}$$

with $z = m_q^2/s$. For zero mass these expressions reduce to equations (2.9).

Next we give the functions appearing in equations (3.2), (3.4) for the QCD $e^+e^- \rightarrow (\gamma^*, Z) \rightarrow b\bar{b}g$ contribution to F_9 . We first decompose $f^{v,1}$, $f^{v,2}$, $f^{a,1}$ and $f^{a,2}$ into sums of imaginary parts of scalar integrals, multiplied by coefficient functions,

$$\begin{aligned}
f^{v(a),1} &= d_{D=6}^{v(a)} \text{Im } D_0^{D=6} \\
&\quad + c_{134}^{v(a),1} \text{Im } C_0(1, 3, 4) + c_{234}^{v(a),1} \text{Im } C_0(2, 3, 4) \\
&\quad + b_{13}^{v(a),1} \text{Im } B_0(1, 3) + b_{24}^{v(a),1} \text{Im } B_0(2, 4) + b_{34}^{v(a),1} \text{Im } B_0(3, 4), \\
f^{v(a),2} &= \tilde{d}_{D=6}^{v(a)} \text{Im } \tilde{D}_0^{D=6} + \tilde{d}'_{D=6}^{v(a)} \text{Im } \tilde{D}'_0^{D=6} \\
&\quad + c_{134}^{v(a),2} \text{Im } C_0(1, 3, 4) + c_{234}^{v(a),2} \text{Im } C_0(2, 3, 4) \\
&\quad + \tilde{c}_{123}^{v(a)} \text{Im } \tilde{C}_0(1, 2, 3) + \tilde{c}_{134}^{v(a)} \text{Im } \tilde{C}_0(1, 3, 4) + \tilde{c}_{234}^{v(a)} \text{Im } \tilde{C}_0(2, 3, 4) \\
&\quad + b_{13}^{v(a),2} \text{Im } B_0(1, 3) + b_{24}^{v(a),2} \text{Im } B_0(2, 4) + b_{34}^{v(a),2} \text{Im } B_0(3, 4) \\
&\quad + \tilde{b}_{24}^{v(a)} \text{Im } \tilde{B}_0(2, 4).
\end{aligned} \tag{II.2}$$

Here B_0 stands generically for a bubble integral, C_0 for a triangle integral, and $D_0^{D=6}$ for a “ $D = 6$ ” box integral; the usual $D = 4$ scalar box integral D_0 has been eliminated in favor of a linear combination of $D_0^{D=6}$ and four C_0 ’s [22].

The explicit formulae for the imaginary parts of the integrals are

$$\begin{aligned}
\text{Im } D_0^{D=6} &= \frac{-\pi}{s} \left[\frac{\rho(1-2x_+^s) + (1-\bar{x})x_+^s \ell^\rho(x_+^s)}{(x_+^s - x_-^s)(x_+^s - x_+^t)(x_+^s - x_-^t)} + \frac{\rho(1-2x_-^s) + (1-\bar{x})x_-^s \ell^\rho(x_-^s)}{(x_-^s - x_+^s)(x_-^s - x_+^t)(x_-^s - x_-^t)} \right. \\
&\quad \left. + \frac{\rho(1-2x_+^t) + (1-x)(1-x_+^t) \ell^\rho(x_+^t)}{(x_+^t - x_+^s)(x_+^t - x_-^s)(x_+^t - x_-^t)} + \frac{\rho(1-2x_-^t) + (1-x)(1-x_-^t) \ell^\rho(x_-^t)}{(x_-^t - x_+^s)(x_-^t - x_-^s)(x_-^t - x_+^t)} \right], \\
\text{Im } C_0(1, 3, 4) &= \frac{-\pi}{s\sqrt{\bar{x}^2 - 4z}} (\ell^\rho(x_+^s) - \ell^\rho(x_-^s)), \\
\text{Im } C_0(2, 3, 4) &= \text{Im } C_0(1, 3, 4)|_{x \leftrightarrow \bar{x}}, \\
\text{Im } B_0(1, 3) &= \frac{\pi(1-\bar{x})}{(1-\bar{x}+z)}, \\
\text{Im } B_0(2, 4) &= \text{Im } B_0(1, 3)|_{x \leftrightarrow \bar{x}}, \\
\text{Im } B_0(3, 4) &= \pi\sqrt{1-4z}, \\
\text{Im } \tilde{D}_0^{D=6} &= \frac{\pi}{2s((x+\bar{x}-1)(1-x)(1-\bar{x})-z(2-x-\bar{x})^2)} \\
&\quad \times \left\{ (x+\bar{x}-1)(1-\bar{x})(1-2\rho')[2\ln(1-\bar{x})-4\ln(1-\rho-\rho')+3\ln(1-\rho')-\ln(\rho')] \right. \\
&\quad \left. + \frac{(1-\bar{x})(\bar{x}(x+\bar{x}-1)-2z(x+\bar{x}))}{\sqrt{\bar{x}^2-4z}} [\ell^\rho(x_+^s) - \ell^\rho(x_-^s)] \right. \\
&\quad \left. + ((x+\bar{x}-1)(1-\bar{x})-2z(2-x-\bar{x})) \left[\ln\left(\frac{z}{1-\bar{x}+z}\right) - \ln\left(\frac{\rho}{1-\rho}\right) + \ln\left(\frac{\rho'}{1-\rho'}\right) \right] \right\}, \\
\text{Im } \tilde{D}'_0^{D=6} &= \text{Im } \tilde{D}_0^{D=6}|_{x \leftrightarrow \bar{x}}, \\
\text{Im } \tilde{C}_0(1, 2, 3) &= \frac{\pi}{s(1-\bar{x})} \ln\left(\frac{z}{1-\bar{x}+z}\right), \\
\text{Im } \tilde{C}_0(1, 3, 4) &= \text{Im } \tilde{C}_0(1, 2, 3)|_{x \leftrightarrow \bar{x}}, \\
\text{Im } \tilde{C}_0(2, 3, 4) &= \frac{\pi}{s(2-x-\bar{x})} \left[\ln\left(\frac{\rho}{1-\rho}\right) - \ln\left(\frac{\rho'}{1-\rho'}\right) \right], \\
\text{Im } \tilde{B}_0(2, 4) &= \pi\sqrt{1-\frac{4z}{x+\bar{x}-1}},
\end{aligned} \tag{II.3}$$

where

$$\begin{aligned}
\rho &= \frac{1-\sqrt{1-4z}}{2}, \\
\rho' &= \frac{1}{2} \left(1 - \sqrt{1 - \frac{4z}{x+\bar{x}-1}} \right), \\
x_\pm^s &= \frac{\bar{x} \pm \sqrt{\bar{x}^2 - 4z}}{2}, \\
x_\pm^t &= 1 - \frac{x \mp \sqrt{x^2 - 4z}}{2}, \\
\ell^\rho(y) &= \ln\left(\frac{(1-y)(y-\rho)}{y(1-y-\rho)}\right).
\end{aligned} \tag{II.4}$$

The coefficient functions are

$$\begin{aligned}
d_{D=6}^v &= \frac{-zs(x-\bar{x})(2-x-\bar{x})}{(1-x)^2(1-\bar{x})^2}, \\
c_{134}^{v,1} &= \left[-\frac{\bar{x}^2-4z}{(1-\bar{x})} - \frac{\bar{x}+2x\bar{x}^2-3x\bar{x}+2x-2\bar{x}^2}{(1-x)(1-\bar{x})} + \frac{3x\bar{x}-7x+2\bar{x}^3-\bar{x}-\bar{x}^2+4}{2(\bar{x}^2-4z)} \right. \\
&\quad \left. + \frac{3\bar{x}(1-\bar{x})(2(1-x-\bar{x})+\bar{x}^2+x\bar{x})}{2(\bar{x}^2-4z)^2} \right] \frac{zs}{2(1-x)}, \\
c_{234}^{v,1} &= -c_{134}^{v,1}|_{x \leftrightarrow \bar{x}}, \\
b_{13}^{v,1} &= \frac{-1}{32(1-x)(1+z-\bar{x})} \left[\frac{(\bar{x}^2-4z)^3}{(1-\bar{x})^2} - \frac{(\bar{x}^2-4z)^2(8+4\bar{x}^2-9\bar{x})}{(1-\bar{x})^2} \right. \\
&\quad + \frac{(\bar{x}^2-4z)(12\bar{x}^4-51\bar{x}^3+44+3x\bar{x}^2-10x\bar{x}-91\bar{x}+92\bar{x}^2+7x)}{2(1-\bar{x})^2} \\
&\quad - \frac{-45\bar{x}^5+8\bar{x}^6-50x\bar{x}^3+16+88\bar{x}^2+109x\bar{x}^2-133\bar{x}^3+106\bar{x}^4+9x\bar{x}^4+36x-104x\bar{x}-38\bar{x}}{2(1-\bar{x})^2} \\
&\quad + \frac{(2-\bar{x})(2\bar{x}^6-3\bar{x}^5+9x\bar{x}^4-13\bar{x}^4+54\bar{x}^3-43x\bar{x}^3-80\bar{x}^2+78x\bar{x}^2+60\bar{x}-64x\bar{x}-16+16x)}{2(\bar{x}^2-4z)(1-\bar{x})} \\
&\quad \left. + \frac{3\bar{x}^2(2-\bar{x})^3(2(1-x-\bar{x})+\bar{x}^2+x\bar{x})}{2(\bar{x}^2-4z)^2} \right], \\
b_{24}^{v,1} &= -b_{13}^{v,1}|_{x \leftrightarrow \bar{x}}, \\
b_{34}^{v,1} &= \frac{4x\bar{x}^2-7x\bar{x}-3\bar{x}^2+2\bar{x}+2\bar{x}^3+2\bar{x}^4+4-4x}{8(1-x)(1-\bar{x})(\bar{x}^2-4z)} \\
&\quad - \frac{4x^2\bar{x}-7x\bar{x}-3x^2+2x+2x^3+2x^4+4-4\bar{x}}{8(1-x)(1-\bar{x})(x^2-4z)} \\
&\quad + \frac{3\bar{x}^2(2(1-x-\bar{x})+\bar{x}^2+x\bar{x})}{8(1-x)(\bar{x}^2-4z)^2} - \frac{3x^2(2(1-x-\bar{x})+x^2+x\bar{x})}{8(1-\bar{x})(x^2-4z)^2} \\
&\quad - \frac{(x-\bar{x})((x+\bar{x})(2(1-x-\bar{x})+x\bar{x})+2z(x+\bar{x}+x\bar{x})+8z^2)}{2(1-x)(1-\bar{x})(x^2-4z)(\bar{x}^2-4z)} \\
&\quad + \frac{(x-\bar{x})(x+\bar{x}-1)}{4(1-x)(1-\bar{x})},
\end{aligned} \tag{II.5}$$

$$\begin{aligned}
d_{D=6}^a &= \frac{-zs(x-\bar{x})(3(1-x-\bar{x})+x^2+x\bar{x}+\bar{x}^2)}{(1-x)^2(1-\bar{x})^2}, \\
c_{134}^{a,1} &= \left[\frac{\bar{x}^2-4z}{(1-\bar{x})} + \frac{-9\bar{x}^2+16\bar{x}-10x\bar{x}+5x\bar{x}^2+7x-9+2x^2\bar{x}-2x^2}{2(1-x)(1-\bar{x})} \right. \\
&\quad \left. - \frac{-10x\bar{x}+5x\bar{x}^2+9x-13\bar{x}^2+11\bar{x}+6\bar{x}^3-6}{2(\bar{x}^2-4z)} + \frac{3\bar{x}(1-\bar{x})^2(2(1-x-\bar{x})+\bar{x}^2+x\bar{x})}{2(\bar{x}^2-4z)^2} \right] \frac{zs}{2(1-x)}, \\
c_{234}^{a,1} &= -c_{134}^{a,1}|_{x \leftrightarrow \bar{x}}, \\
b_{13}^{a,1} &= \frac{-1}{32(1-x)(1+z-\bar{x})} \left[-\frac{(\bar{x}^2-4z)^3}{(1-\bar{x})^2} + \frac{(\bar{x}^2-4z)^2(2x\bar{x}+9+9\bar{x}^2-18\bar{x})}{2(1-\bar{x})^2} \right. \\
&\quad \left. - \frac{(\bar{x}^2-4z)(26+18\bar{x}^4-73\bar{x}^3-27x\bar{x}^2+9x\bar{x}^3+114\bar{x}^2-91\bar{x}-21x+43x\bar{x})}{2(1-\bar{x})^2} \right. \\
&\quad \left. + \left(-60x+382\bar{x}^2-297x\bar{x}^2+208x\bar{x}+20\bar{x}^6-479\bar{x}^3+332\bar{x}^4 \right. \right. \\
&\quad \left. \left. + 223x\bar{x}^3-125\bar{x}^5-87x\bar{x}^4+15x\bar{x}^5+24-158\bar{x} \right) \frac{1}{2(1-\bar{x})^2} \right. \\
&\quad \left. - \left(12\bar{x}^6-67\bar{x}^5+11x\bar{x}^5-60x\bar{x}^4+161\bar{x}^4-212\bar{x}^3+131x\bar{x}^3 \right. \right. \\
&\quad \left. \left. - 150x\bar{x}^2+172\bar{x}^2-84\bar{x}+88x\bar{x}+16-16x \right) \frac{2-\bar{x}}{2(1-\bar{x})(\bar{x}^2-4z)} \right. \\
&\quad \left. + \frac{3\bar{x}^2(1-\bar{x})(2-\bar{x})^3(2(1-x-\bar{x})+\bar{x}^2+x\bar{x})}{2(\bar{x}^2-4z)^2} \right], \\
b_{24}^{a,1} &= -b_{13}^{a,1}|_{x \leftrightarrow \bar{x}}, \\
b_{34}^{a,1} &= -\frac{23\bar{x}^2+6x\bar{x}^3-4-19x\bar{x}^2-8\bar{x}+7\bar{x}^4-20\bar{x}^3+13x\bar{x}+4x}{8(1-x)(1-\bar{x})(\bar{x}^2-4z)} \\
&\quad + \frac{23x^2+6x^3\bar{x}-4-19x^2\bar{x}-8x+7x^4-20x^3+13x\bar{x}+4\bar{x}}{8(1-x)(1-\bar{x})(x^2-4z)} \\
&\quad + \frac{3\bar{x}^2(1-\bar{x})(2(1-x-\bar{x})+\bar{x}^2+x\bar{x})}{8(1-x)(\bar{x}^2-4z)^2} - \frac{3x^2(1-x)(2(1-x-\bar{x})+x^2+x\bar{x})}{8(1-\bar{x})(x^2-4z)^2} \\
&\quad + \frac{(x-\bar{x})\left(-(x+\bar{x})(2(1-x-\bar{x})+x\bar{x})+2z(x+\bar{x}-2(x^2+\bar{x}^2)-3x\bar{x})+8z^2 \right)}{2(1-x)(1-\bar{x})(x^2-4z)(\bar{x}^2-4z)} \\
&\quad - \frac{(x-\bar{x})(4(x+\bar{x})-1)}{8(1-x)(1-\bar{x})},
\end{aligned} \tag{II.6}$$

$$\begin{aligned}
\tilde{d}_{D=6}^v &= \left[-(x + \bar{x} - 1) - \frac{z(-3x + 2x^2 + \bar{x} - \bar{x}^2 + x\bar{x})}{(x + \bar{x} - 1)(1 - \bar{x})} + \frac{4z^2(2 - x - \bar{x})}{(x + \bar{x} - 1)(1 - \bar{x})} \right] \frac{s}{2(1 - x)(1 - \bar{x})}, \\
\tilde{d}'_{D=6}{}^v &= -\tilde{d}_{D=6}^v|_{x \leftrightarrow \bar{x}}, \\
c_{134}^{v,2} &= \left[\frac{(2 - x - \bar{x})(\bar{x}^2 - 4z)^2}{(x + \bar{x} - 1)(1 - \bar{x})} + \frac{(\bar{x}^2 - 4z)(-3 + 6\bar{x} + 2x - 8\bar{x}^2 + 3\bar{x}^3 + 3x\bar{x}^2 - 3x\bar{x})}{(x + \bar{x} - 1)(1 - \bar{x})} \right. \\
&\quad + \frac{(3(1 - x - \bar{x}) + \bar{x}^3 + x\bar{x})(3\bar{x} - 2 + 2x)}{(x + \bar{x} - 1)(1 - \bar{x})} \\
&\quad - \frac{-5\bar{x} - 6x\bar{x} + 2\bar{x}^2 - 5x - 5\bar{x}^3 + 4 + 6\bar{x}^4 + 3x\bar{x}^2}{2(1 - \bar{x})} \\
&\quad - \frac{\bar{x}(\bar{x}^4 + \bar{x}^3 - 7\bar{x}^2 + 3x\bar{x}^2 + 10\bar{x} - 8x\bar{x} - 3 + 3x)}{(\bar{x}^2 - 4z)} \\
&\quad \left. - \frac{3\bar{x}^3(1 - \bar{x})(2(1 - x - \bar{x}) + \bar{x}^2 + x\bar{x})}{2(\bar{x}^2 - 4z)^2} \right] \frac{s}{8(1 - x)}, \\
c_{234}^{v,2} &= -c_{134}^{v,2}|_{x \leftrightarrow \bar{x}}, \\
\tilde{c}_{123}^v &= \frac{-zs(x + 4z)}{2(x + \bar{x} - 1)(1 - x)(1 - \bar{x})}, \\
\tilde{c}_{134}^v &= -\tilde{c}_{123}^v|_{x \leftrightarrow \bar{x}}, \\
\tilde{c}_{234}^v &= \frac{-zs(x - \bar{x})}{(1 - x)^2(1 - \bar{x})^2} \left[\frac{5(1 - x - \bar{x}) + x^2 + 3x\bar{x} + \bar{x}^2}{2 - x - \bar{x}} + \frac{2z(2 - x - \bar{x})}{x + \bar{x} - 1} \right], \\
b_{13}^{v,2} &= \frac{1}{32(1 - x)(1 + z - \bar{x})} \left[\frac{(\bar{x}^2 - 4z)^3}{(1 - \bar{x})^2} - \frac{(\bar{x}^2 - 4z)^2(4\bar{x}^2 - 9\bar{x} + 9)}{(1 - \bar{x})^2} \right. \\
&\quad + \frac{(\bar{x}^2 - 4z)(12\bar{x}^4 - 51\bar{x}^3 + 48 + 3x\bar{x}^2 - 10x\bar{x} - 91\bar{x} + 92\bar{x}^2 + 7x)}{2(1 - \bar{x})^2} \\
&\quad - \frac{-45\bar{x}^5 + 8\bar{x}^6 - 50x\bar{x}^3 + 24\bar{x}^2 + 109x\bar{x}^2 - 101\bar{x}^3 + 100\bar{x}^4 + 9x\bar{x}^4 + 36x - 104x\bar{x} + 18\bar{x}}{2(1 - \bar{x})^2} \\
&\quad + \frac{(2 - \bar{x})(2\bar{x}^6 - 3\bar{x}^5 + 9x\bar{x}^4 - 17\bar{x}^4 + 74\bar{x}^3 - 43x\bar{x}^3 - 112\bar{x}^2 + 78x\bar{x}^2 + 76\bar{x} - 64x\bar{x} - 16 + 16x)}{2(1 - \bar{x})(\bar{x}^2 - 4z)} \\
&\quad \left. + \frac{3\bar{x}^2(2 - \bar{x})^3(2(1 - x - \bar{x}) + \bar{x}^2 + x\bar{x})}{2(\bar{x}^2 - 4z)^2} \right], \\
b_{24}^{v,2} &= -b_{13}^{v,2}|_{x \leftrightarrow \bar{x}},
\end{aligned} \tag{II.7}$$

$$\begin{aligned}
b_{34}^{v,2} &= -\frac{4x\bar{x}^2 - 7x\bar{x} - 3\bar{x}^2 + 2\bar{x} + 2\bar{x}^3 + 2\bar{x}^4 + 4 - 4x}{8(1-x)(1-\bar{x})(\bar{x}^2 - 4z)} \\
&+ \frac{4x^2\bar{x} - 7x\bar{x} - 3x^2 + 2x + 2x^3 + 2x^4 + 4 - 4\bar{x}}{8(1-x)(1-\bar{x})(x^2 - 4z)} \\
&- \frac{3\bar{x}^2(2(1-x-\bar{x}) + \bar{x}^2 + x\bar{x})}{8(1-x)(\bar{x}^2 - 4z)^2} + \frac{3x^2(2(1-x-\bar{x}) + x^2 + x\bar{x})}{8(1-\bar{x})(x^2 - 4z)^2} - \frac{(x-\bar{x})(x+\bar{x}-1)}{4(1-x)(1-\bar{x})} \\
&+ \left(-2(x^4 + \bar{x}^4) + (x^3 + \bar{x}^3)(x\bar{x} + 10) - (x^2 + \bar{x}^2)(13x\bar{x} + 16) + (x + \bar{x})(3x^2\bar{x}^2 + 38x\bar{x} + 8) \right. \\
&- 23x^2\bar{x}^2 - 36x\bar{x} + 2z \left(3(x^3 + \bar{x}^3) + x\bar{x}(x^2 + \bar{x}^2) + (x + \bar{x})(5x\bar{x} - 12(x + \bar{x}) + 20) + 2x^2\bar{x}^2 - 8 \right) \\
&\left. + 8z^2 \left((x + \bar{x})(x + \bar{x} - 4) + 2 \right) \right) \frac{x - \bar{x}}{2(2 - x - \bar{x})^2(1-x)(1-\bar{x})(x^2 - 4z)(\bar{x}^2 - 4z)}, \\
\tilde{b}_{24}^v &= \frac{x - \bar{x}}{2(2 - x - \bar{x})^2(1-x)(1-\bar{x})},
\end{aligned} \tag{II.8}$$

$$\begin{aligned}
\tilde{d}_{D=6}^a &= \left[(x + \bar{x} - 1)^2 - \frac{z(2x^3 - 7x^2 + x^2\bar{x} + 16x - 11x\bar{x} - x\bar{x}^2 + 20\bar{x} - 8\bar{x}^2 - 12)}{(1 - \bar{x})} \right. \\
&\quad + \frac{4z^2(14x - 6x^2 + x^3 + 16\bar{x} - 10x\bar{x} - 6\bar{x}^2 + x^2\bar{x} - 10)}{(x + \bar{x} - 1)(1 - \bar{x})} - \left. \frac{16z^3(2 - x - \bar{x})}{(x + \bar{x} - 1)(1 - \bar{x})} \right] \\
&\quad \times \frac{s}{2(1 - x)(1 - \bar{x})(1 + 4z - x - \bar{x})}, \\
\tilde{d}'_{D=6}^a &= -\tilde{d}_{D=6}^a|_{x \leftrightarrow \bar{x}}, \\
c_{134}^{a,2} &= \left[\frac{(\bar{x}^2 - 4z)^2}{(1 - \bar{x})} - \frac{(\bar{x}^2 - 4z)(-6x - 8\bar{x} + 2x\bar{x} + 1 + 7\bar{x}^2)}{2(1 - \bar{x})} \right. \\
&\quad + \frac{-29\bar{x}^3 + 11\bar{x}^4 + 19x\bar{x} + 7x\bar{x}^3 - 25x\bar{x}^2 - 11\bar{x} + 3x + 29\bar{x}^2 - 2}{2(1 - \bar{x})} \\
&\quad + \frac{\bar{x}(9\bar{x}^4 + 8x\bar{x}^3 - 27\bar{x}^3 - 26x\bar{x}^2 + 34\bar{x}^2 - 16\bar{x} + 20x\bar{x} + 2x - 2)}{2(\bar{x}^2 - 4z)} \\
&\quad - \frac{3\bar{x}^3(1 - \bar{x})^2(2(1 - x - \bar{x}) + \bar{x}^2 + x\bar{x})}{2(\bar{x}^2 - 4z)^2} + \frac{(\bar{x}^2 - 4z)^3}{(x + \bar{x} - 1)(1 + 4z - x - \bar{x})(1 - \bar{x})} \\
&\quad + \frac{(\bar{x}^2 - 4z)^2(4x - 5\bar{x}^2 + 8\bar{x} + x^2 - 6)}{(x + \bar{x} - 1)(1 + 4z - x - \bar{x})(1 - \bar{x})} \\
&\quad + \left(3x^2\bar{x} + 2x^3 - 25\bar{x} + 21x\bar{x} - 23\bar{x}^3 - 17x + 33\bar{x}^2 + 5x^2 + 10 + 8\bar{x}^4 - x\bar{x}^3 - 4x^2\bar{x}^2 - 11x\bar{x}^2 \right) \\
&\quad \times \frac{(\bar{x}^2 - 4z)}{(x + \bar{x} - 1)(1 + 4z - x - \bar{x})(1 - \bar{x})} \\
&\quad - \left(11x^2\bar{x}^2 + 50x\bar{x} - 2x\bar{x}^5 + 52\bar{x}^2 + 46\bar{x}^4 + 6 + 18x^2 + 42x\bar{x}^3 - 67x\bar{x}^2 - 5x^2\bar{x}^4 + 5\bar{x}^6 \right. \\
&\quad \left. - 25\bar{x} + 4x^3\bar{x}^2 - 6x^3 - 9x\bar{x}^4 - 21\bar{x}^5 + 6x^2\bar{x}^3 - 18x - 25x^2\bar{x} - 62\bar{x}^3 \right) \\
&\quad \times \frac{1}{(x + \bar{x} - 1)(1 + 4z - x - \bar{x})(1 - \bar{x})} \\
&\quad + \left. \frac{\bar{x}(1 - \bar{x})(x + \bar{x} - 1 - \bar{x}^2)(2x\bar{x} + 4x - \bar{x}^2 + 2\bar{x} - 4)}{(1 + 4z - x - \bar{x})(\bar{x}^2 - 4z)} \right] \frac{s}{8(1 - x)}, \\
c_{234}^{a,2} &= -c_{134}^{a,2}|_{x \leftrightarrow \bar{x}}, \\
\tilde{c}_{123}^a &= \left[-\frac{2x^2 + 2x\bar{x} - 5x - 5\bar{x} + 4 + \bar{x}^2}{2(1 - x)(1 - \bar{x})} \right. \\
&\quad - \frac{z(5x\bar{x}^2 + 5x^2\bar{x} - 6x^2 - 10 + 3\bar{x}^3 + 23\bar{x} - 18x\bar{x} + x^3 - 16\bar{x}^2 + 13x)}{(x + \bar{x} - 1)(1 - x)(1 - \bar{x})^2} \\
&\quad + \left. \frac{4z^2(2x\bar{x} + 4 + x^2 - 3x - 5\bar{x} + \bar{x}^2)}{(x + \bar{x} - 1)(1 - x)(1 - \bar{x})^2} \right] \frac{zs}{1 + 4z - x - \bar{x}}, \\
\tilde{c}_{134}^a &= -\tilde{c}_{123}^a|_{x \leftrightarrow \bar{x}},
\end{aligned} \tag{II.9}$$

$$\begin{aligned}
\tilde{c}_{234}^a &= \left[-\frac{2(x^4 + \bar{x}^4) - 15(x^3 + \bar{x}^3) + (x^2 + \bar{x}^2)(7x\bar{x} + 43) - (x + \bar{x})(43x\bar{x} + 52) + 10x^2\bar{x}^2 + 84x\bar{x} + 22}{2(2 - x - \bar{x})} \right. \\
&\quad + \frac{2z(x^4 + \bar{x}^4 - 9(x^3 + \bar{x}^3) + 3(x^2 + \bar{x}^2)(x\bar{x} + 10) - 5(x + \bar{x})(8 + 5x\bar{x}) + 4x^2\bar{x}^2 + 58x\bar{x} + 18)}{(2 - x - \bar{x})(x + \bar{x} - 1)} \\
&\quad \left. + \frac{8z^2(2 - x - \bar{x})}{x + \bar{x} - 1} \right] \frac{z(x - \bar{x})}{(1 - x)^2(1 - \bar{x})^2} \frac{s}{1 + 4z - x - \bar{x}}, \\
b_{13}^{a,2} &= \left[-\frac{(x - \bar{x})(\bar{x}^2 - 4z)^3}{(1 - \bar{x})^3} + \frac{(\bar{x}^2 - 4z)^2(4x + x\bar{x}^2 - 6\bar{x}^3 - 21\bar{x} + 5 + 19\bar{x}^2 - 2x\bar{x})}{(1 - \bar{x})^3} \right. \\
&\quad + \frac{(\bar{x}^2 - 4z)(-28x\bar{x}^3 + 207\bar{x}^3 + 62x\bar{x}^2 + 6x\bar{x}^4 + 197\bar{x} + 21x + 15\bar{x}^5 - 277\bar{x}^2 - 64x\bar{x} - 54 - 85\bar{x}^4)}{(1 - \bar{x})^3} \\
&\quad - \left(60x - 72 + 1293\bar{x}^3 - 1055\bar{x}^4 + 523\bar{x}^5 - 520x\bar{x}^3 + 306x\bar{x}^4 - 98x\bar{x}^5 - 956\bar{x}^2 \right. \\
&\quad \left. + 505x\bar{x}^2 - 268x\bar{x} - 149\bar{x}^6 + 19\bar{x}^7 + 398\bar{x} + 14x\bar{x}^6 \right) \frac{1}{(1 - \bar{x})^3} \\
&\quad - \left(12\bar{x}^6 + 11x\bar{x}^5 - 71\bar{x}^5 + 185\bar{x}^4 - 60x\bar{x}^4 - 264\bar{x}^3 + 131x\bar{x}^3 - 150x\bar{x}^2 \right. \\
&\quad \left. + 220\bar{x}^2 - 100\bar{x} + 88x\bar{x} + 16 - 16x \right) \frac{2 - \bar{x}}{(1 - \bar{x})(\bar{x}^2 - 4z)} \\
&\quad \left. + \frac{3\bar{x}^2(1 - \bar{x})(2 - \bar{x})^3(2(1 - x - \bar{x}) + \bar{x}^2 + x\bar{x})}{(\bar{x}^2 - 4z)^2} \right] \frac{1}{64(1 - x)(1 + z - \bar{x})}, \\
b_{24}^{a,2} &= -b_{13}^{a,2}|_{x \leftrightarrow \bar{x}}, \\
b_{34}^{a,2} &= \frac{23\bar{x}^2 + 6x\bar{x}^3 - 4 - 19x\bar{x}^2 - 8\bar{x} + 7\bar{x}^4 - 20\bar{x}^3 + 13x\bar{x} + 4x}{8(1 - x)(1 - \bar{x})(\bar{x}^2 - 4z)} \\
&\quad - \frac{23x^2 + 6x^3\bar{x} - 4 - 19x^2\bar{x} - 8x + 7x^4 - 20x^3 + 13x\bar{x} + 4\bar{x}}{8(1 - x)(1 - \bar{x})(x^2 - 4z)} \\
&\quad - \frac{3\bar{x}^2(1 - \bar{x})(2(1 - x - \bar{x}) + \bar{x}^2 + x\bar{x})}{8(1 - x)(\bar{x}^2 - 4z)^2} + \frac{3x^2(1 - x)(2(1 - x - \bar{x}) + x^2 + x\bar{x})}{8(1 - \bar{x})(x^2 - 4z)^2} \\
&\quad + \left(-2(x^4 + \bar{x}^4) + (x^3 + \bar{x}^3)(x\bar{x} + 10) - (x^2 + \bar{x}^2)(13x\bar{x} + 16) + (x + \bar{x})(3x^2\bar{x}^2 + 38x\bar{x} + 8) \right. \\
&\quad - 23x^2\bar{x}^2 - 36x\bar{x} \\
&\quad - 2z(-2(x^4 + \bar{x}^4) + 5(x^3 + \bar{x}^3) + (x^2 + \bar{x}^2)(-5x\bar{x} + 4) \\
&\quad \left. + (x + \bar{x})(3x\bar{x} - 20) - 6x^2\bar{x}^2 + 24x\bar{x} + 8) \right) \\
&\quad - 8z^2 \left(3(x + \bar{x})(x + \bar{x} - 4) + 14 \right) \frac{x - \bar{x}}{2(2 - x - \bar{x})^2(1 - x)(1 - \bar{x})(x^2 - 4z)(\bar{x}^2 - 4z)} \\
&\quad + \frac{(x - \bar{x})(4(x + \bar{x}) - 1)}{8(1 - x)(1 - \bar{x})}, \\
\tilde{b}_{24}^a &= \tilde{b}_{24}^v.
\end{aligned}$$

(II.10)

References

- [1] K. Abe et al., Phys. Rev. Lett. 73:25 (1994).
- [2] ALEPH Collaboration, DELPHI Collaboration, L3 Collaboration, OPAL Collaboration; LEP Electroweak Working Group, CERN-PPE-94-187.
- [3] K. Fabricius, J.G. Körner, G. Kramer, G. Schierholz and I. Schmitt, Phys. Lett. 94B:207 (1980).
- [4] K. Fabricius, G. Kramer, G. Schierholz and I. Schmitt, Phys. Rev. Lett. 45:867 (1980).
- [5] A. De Rújula, J.M. Kaplan and E. de Rafael, Nucl. Phys. B35:365 (1971);
A. De Rújula, R. Petronzio and B. Lautrup, Nucl. Phys. B146:50 (1978).
- [6] For example: J. F. Donoghue and G. Valencia, Phys. Rev. Lett. 58:451 (1987); M. B. Gavela, F. Iddir, A. Le Yaouanc, L. Oliver, O. Pene and J. C. Raynal, Phys. Rev. D39:1870 (1989); J. Bernabéu and N. Rius, Phys. Lett. B232:127 (1989); M. Kamionkowski, Phys. Rev. D41:1672 (1990); D. Atwood, S. Bar-Shalom and A. Soni, Phys. Rev. D51:1034 (1995).
- [7] W. Bernreuther, U. Löw, J.P. Ma and O. Nachtmann, Z. Phys. C43:117 (1989).
- [8] A. Bilal, E. Massó and A. De Rújula, Nucl. Phys. B355:549 (1991) .
- [9] O. Nachtmann, Nucl. Phys. B127:314 (1977);
A.V. Efremov, Sov. J. Nucl. Phys. 28:83 (1978);
R.H. Dalitz, G.R. Goldstein and R. Marshall, Z. Phys. C42:441 (1989);
A.V. Efremov, L. Mankiewicz and N.A. Törnqvist, Phys. Lett. B284:394 (1992).
- [10] J.P. Ralston and B. Pire, in *Proc. of 5th Intl. Symp. on High Energy Spin Physics, Upton, N.Y.*, published in BNL Spin Sympos. (1982); Phys. Rev. D28:260 (1983).
- [11] R. Carlitz and R. Willey, Phys. Rev. D45:2323 (1992).
- [12] K. Hagiwara, K. Hikasa and N. Kai, Phys. Rev. D27:84 (1983).
- [13] J.G. Körner and G. Schuler, Z. Phys. C26:559 (1985).
- [14] K. Hagiwara, T. Kuruma and Y. Yamada, Nucl. Phys. B358:80 (1991).
- [15] C. Carone and H. Murayama, Phys. Rev. Lett. 74:3122 (1995); Phys. Rev. D52:484 (1995), hep-ph/9501220.
- [16] D. Bailey and S. Davidson, Phys. Lett. 348B:185 (1995).
- [17] E.L. Bratkovskaya, E.A. Kuraev, Z.K. Silagadze and O.V. Terayaev, Phys. Lett. B338:471 (1994), hep-ph/9412230.
- [18] H. Olsen and J. Stav, Phys. Rev. D50:6775 (1994).
- [19] D. Atwood and A. Soni, Phys. Rev. D45:2405 (1992).
- [20] K. Abe et al., preprint SLAC-PUB-6969, to be published in Phys. Rev. Lett.
- [21] Z. Kunszt, A. Signer and Z. Trócsányi, Nucl. Phys. B420:550 (1994).

- [22] Z. Bern, L. Dixon and D.A. Kosower, Phys. Lett. 302B:299 (1993); erratum *ibid.* 318:649 (1993); Nucl. Phys. B412:751 (1994).

Figure Captions

Figure 1:

Sample Feynman diagram for the QCD rescattering contribution, with $m_q \neq 0$ required for a nonvanishing result.

Figure 2:

Triangle diagram for QCD rescattering contribution via quark annihilation; again $m_{q'} \neq 0$ is required for a nonvanishing result.

Figure 3:

Sample diagram for electroweak rescattering contribution.

Figure 4:

Sample diagram for contribution of $\gamma\gamma$ and γZ intermediate states.

Figure 5:

Sample diagram for contribution from real $\gamma\gamma$ initial state.

Figure 6:

Definition of the angles θ , ϕ and $\theta_n^{(q\bar{q})}$ for $e^+e^- \rightarrow q\bar{q}g$. The unit vector \mathbf{n} is the (signed) normal to the $q\bar{q}g$ plane.

Figure 7:

$\langle \cos \theta_n \rangle$ from QCD rescattering, normalized for b -final states only, as a function of the center-of-mass energy, for $y_{\text{cut}} = 0.04$. The dotted line gives the contribution of the vector component of the result. The one loop running of α_s is included.

Figure 8:

QCD (dotted line), W -exchange (dot-dashes) and Z -exchange (dashes) contributions to $\langle \cos \theta_n \rangle$ as functions of the center-of-mass energy, for $y_{\text{cut}} = 0.04$. The one loop running of α_s is included. The solid line gives the sum of the three contributions.

Figure 9:

QCD (solid line), W -exchange (dot-dashes) and Z -exchange (dashes) contributions to the signal-to-noise ratio, divided by the square-root of the number of 2-jet events, for $\langle \cos \theta_n \rangle$, as functions of y_{cut} at the Z .

Figure 10:

B boson exchange contribution to $\langle \cos \theta_n \rangle$ as a function of $\xi \equiv M_B^2/M_Z^2$, with (dashed line) and without (solid line) gluon identification, at the Z , for $\alpha_B = 0.2/9$ and $y_{\text{cut}} = 0.04$.

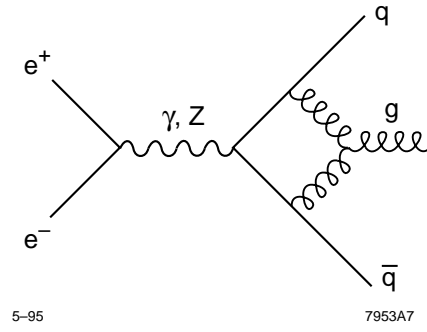


Fig. 1

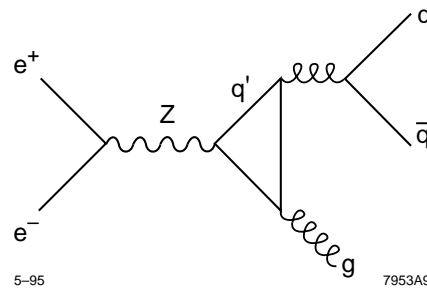


Fig. 2

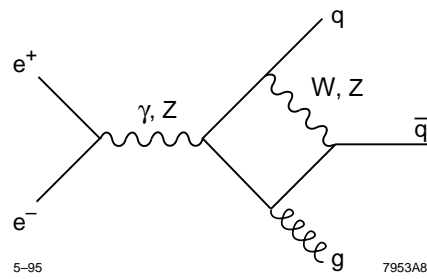


Fig. 3

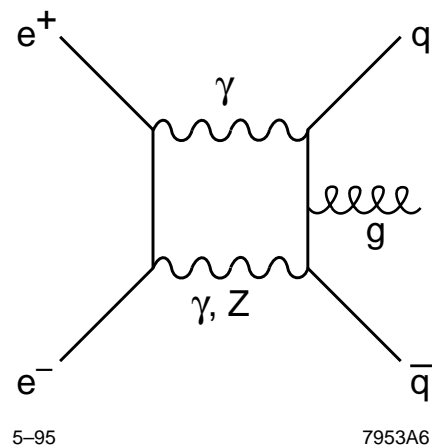


Fig. 4

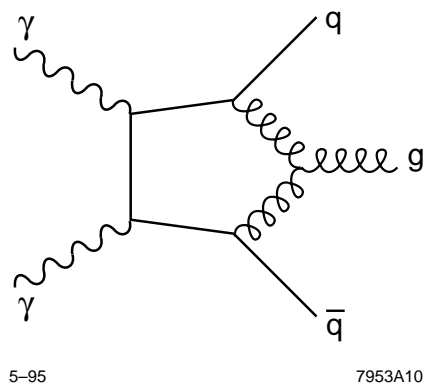
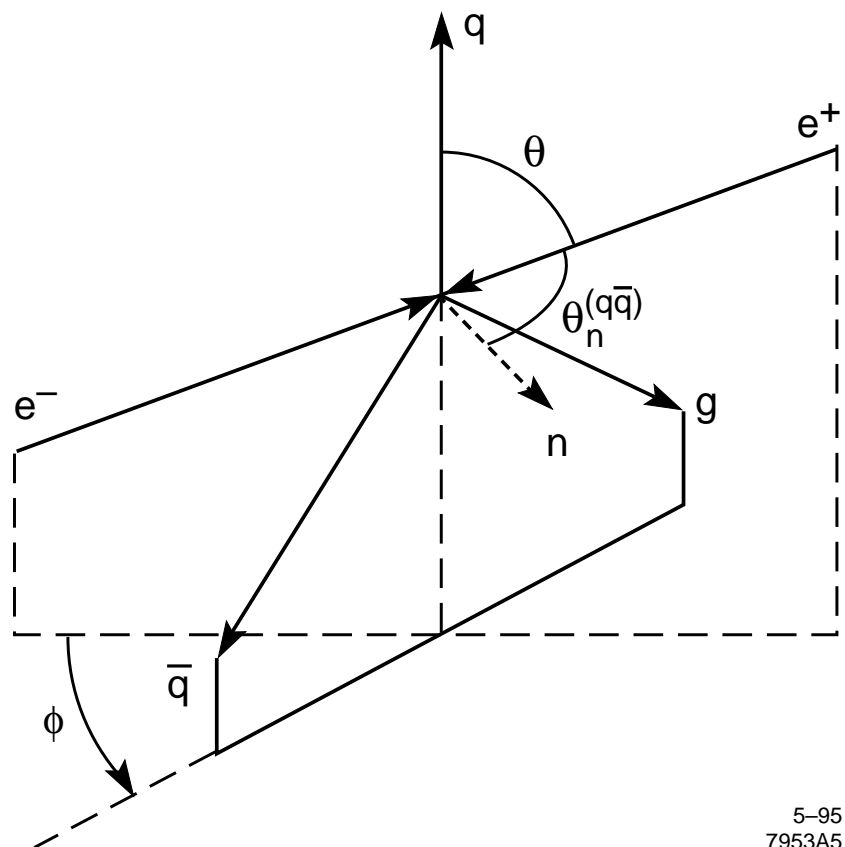


Fig. 5



5-95
7953A5

Fig. 6

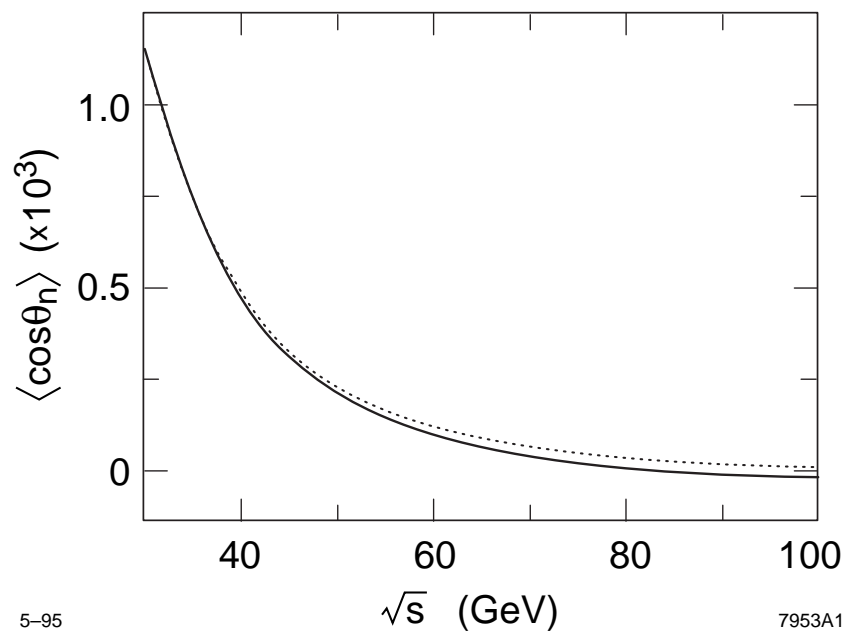


Fig. 7

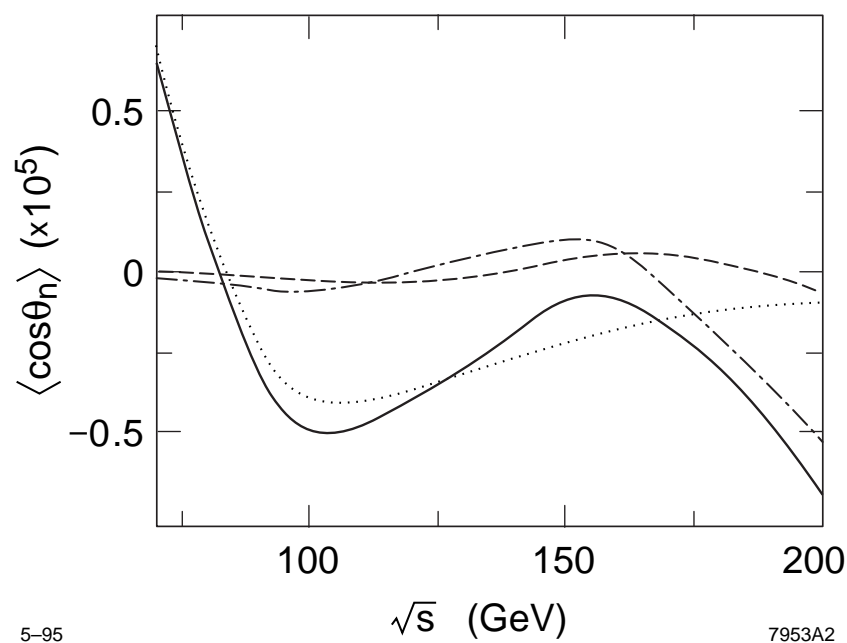


Fig. 8

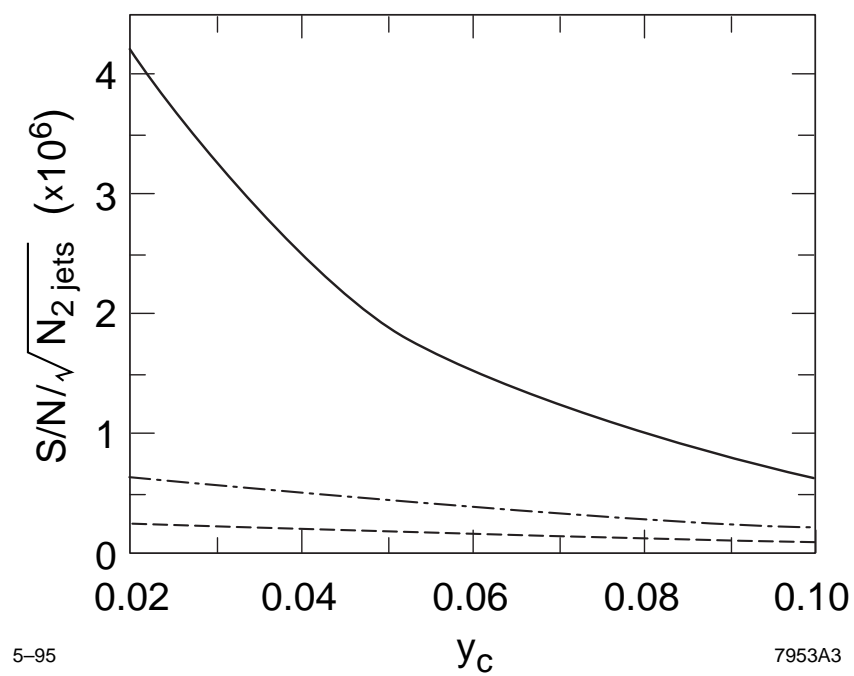


Fig. 9

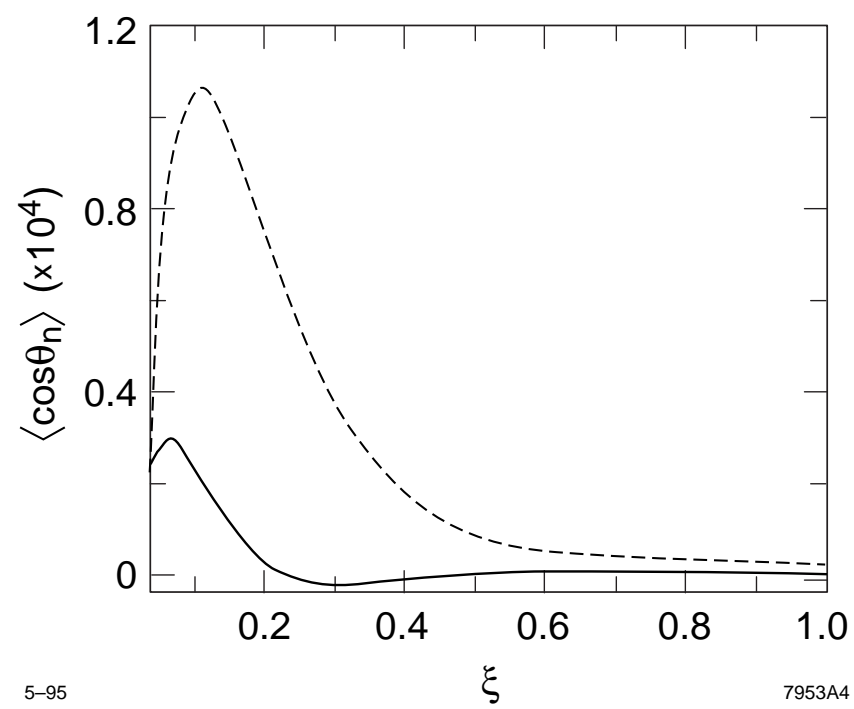


Fig. 10